JOC The Journal of Organic Chemistry

UNIVERSITY OF EXETER

Subscriber access provided by the University of Exeter

Article

Hetero-Diels-Alder Reactions of Quinone Methides: the origin of the #-regioselectivity of 3-methylene-1,2,4-naphthotriones

Maicon Delarmelina, Sabrina B Ferreira, Fernando de C. da Silva, Vitor F. Ferreira, and José Walkimar de M. Carneiro

J. Org. Chem., **Just Accepted Manuscript** • DOI: 10.1021/acs.joc.0c00215 • Publication Date (Web): 05 May 2020

Downloaded from pubs.acs.org on May 8, 2020

is published by the American Chemical Society. 1155 Sixteenth Street N.W., Washington, DC 20036

Hetero-Diels-Alder Reactions of Quinone Methides: the origin of the α-regioselectivity of 3-methylene-1,2,4-naphthotriones

Maicon Delarmelina[a,b], Sabrina B. Ferreira[c], Fernando de C da Silva[a], Vitor F. Ferreira[a,d], José Walkimar de M. Carneiro[a,*]

[a]Instituto de Química, Universidade Federal Fluminense, Niterói, Rio de Janeiro, 24020-141, Brazil. E-mail: jose_walkimar@id.uff.br.

[b]School of Chemistry, Cardiff University, Main Building, Park Place, Cardiff, CF10 3AT, UK.

[c]Instituto de Química, Universidade Federal do Rio de Janeiro, Rio de Janeiro, 21941-909, Brazil.

[d]Faculdade de Farmácia, Universidade Federal Fluminense, Niterói, Rio de Janeiro, 24241-002, Brazil.

ABSTRACT

The regioselective formation of α- and β-lapachone via Hetero-Diels-Alder reactions was investigated by experimental and computational approaches. The experimentally observed α-selectivity was explored in detail, revealing that lower energy barrier for formation of α-lapachone is a result of lower Pauli repulsion throughout the reaction path, when compared to the β-isomer. By comparing equivalent points on both α- and β-lapachone Potential Energy Surfaces (PES) according to the Activation Strain Model (ASM) and Energy Decomposition Analysis (EDA), we were able to demonstrate that the Pauli repulsion term increases more significantly when going from reactants to $\mathbf{TS_\beta}$ than to $\mathbf{TS_\alpha}$, resulting in lower interaction energy in the early stages of the reaction path and in a later transition state for β-lapachone. Moreover, we confirmed that regio- and diastereoselectivity trends previously reported for other quinone methide intermediates are also observed for 3-methylene-1,2,4-naphthotriones, such as small *endo*/*exo* diastereoselectivity, as well as pronounced *ortho*/*meta* regioselectivity for reactions performed with dienophile containing electron-releasing groups. The results presented here provide deeper understanding of the reactivity of quinone methide derivatives, aiding future rational design of reaction condition, structural modification of possible

quinone methide intermediates, and the development of more selective synthetic routes for quinone derivatives.

INTRODUCTION

The quinone methide intermediate **1a** (X = O, **Figure 1**) has been widely explored in the last decades as a versatile synthon in organic synthesis, and more recently inspirational applications were shown in asymmetric[1-4] and natural product synthesis[5,6], in the preparation of bioactive derivatives[7-12], synthesis of heterocycles[13], free-metal catalysis[14], photochemical reactions[15], and biomedicine[16-18]. This class of intermediate is usually obtained *in situ* and it can also be found as dimethane- (**1b**, X = C, **Figure 1**), aza- (**1c**, X = N, **Figure 1**) and thio- (**1d**, X = S, **Figure 1**) congeners, as well as *ortho*- (**1**, **Figure 1**) and *para*-isomers (**2**, **Figure 1**).

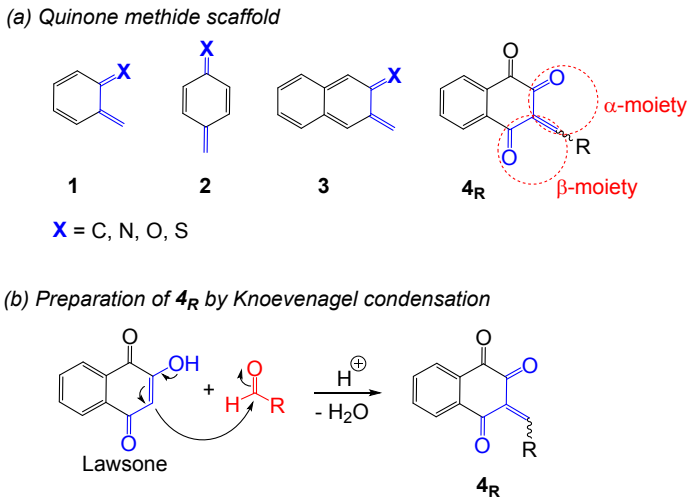

Figure 1. Quinone methide derivatives and formation of $\mathbf{4_R}$ by Knoevenagel condensation.

Amongst the available methodologies for the *in situ* preparation of quinone methide intermediates, one of the simplest and most efficient one is the Knoevenagel condensation (**Figure 1b**). This methodology has been extensively explored by our group, yielding the intermediate 3-methylene-1,2,4-naphthotriones $\mathbf{4_R}$ and allowing the preparation of large set of bioactive pyran naphthoquinone derivatives by hetero-Diels-alder reactions[19-23]. The intermediate $\mathbf{4_R}$ presents increased complexity when compared to the parent quinone methide **1**, as now two almost-symmetrical reaction sites are present:

the α- and β-moieties (**Figure 1a**). Such feature is very convenient for the synthesis of natural products and bioactive compounds since two regioisomers (α- and β-lapachones) can be formed, depending on the reaction conditions employed.

In an important contribution to the rationalization of the regio- and diastereoselectivity of the reaction of **1** as diene in hetero-Diels-Alder reactions, Wang and coworkers[24] (**Figure 2a**) investigated the alternative reaction channels by DFT methods (B3LYP/6-31G(d,p)) and observed that: (i) *meta* isomers are kinetically disfavored against the *ortho* isomers, for which *ortho* transition states are more asynchronous than *meta* transition states; (ii) reactivity, *ortho* selectivity, and asynchronicity of such processes are enhanced by electron-releasing groups bonded to the dienophile fragment; (iii) solvent effect increases the asynchronicity of the transition state structure, reducing the energy barrier for the hetero-Diels-Alder reaction; and, finally, (iv) charge separation in the transition state can lead to distinct mechanisms, ranging from an asynchronous concerted to a zwitterionic transition state[24].

To the best of our knowledge, one of the few mechanistic investigations involving the 3-methylene-1,2,4-naphthotriones $\mathbf{4_R}$ were performed by Peng and coworkers (**Figure 2b**)[25]. Peng investigated the formation of siloxy-containing α-lapachones in a regioselective reaction between $\mathbf{4_R}$ and a set of silyl enol ethers. Analysis of the transition state structures obtained by DFT methods (B3LYP/6-31G(d)) confirmed their zwitterionic character.

Later, our own group investigated the reactivity of $\mathbf{4_R}$ in the preparation of xanthene derivatives from lawsone (**Figure 2c**)[12]. We have shown that, depending on the chosen reaction conditions, the concerted hetero-Diels-Alder reaction is replaced by a two-step process, in which the first step is a Michael addition with formation of an open intermediate (experimentally isolated), followed by the cyclization/dehydration process in acidic conditions. Under these reaction conditions, *ortho,para*-xanthene derivatives were exclusively obtained[12].

Herein we report our theoretical and experimental investigation on the α/β-regioselectivity of hetero-Diels-Alder reaction between the quinone methide $\mathbf{4_H}$ and a set of representative dienophiles (ethene, propene, styrene, methoxyethene, cyanoethene, cyclopentadiene and ethynyl benzene). Using a

new approach for describing the reaction coordinate, we were able to determine quantitatively earlier or later transition state structures involved in the formation of the α/β-isomers and to rationalize the observed regioselectivity for these reactions. Energy Decomposition Analysis (EDA) and Activation Strain Model (ASM) were instrumental for exploring the reaction progress along the reaction coordinate up to the formation of the transition state structures. For the first time, the distinct energy barriers for the formation of α and β-lapachone from 3-methylene-1,2,4-naphthotriones were rationalized.

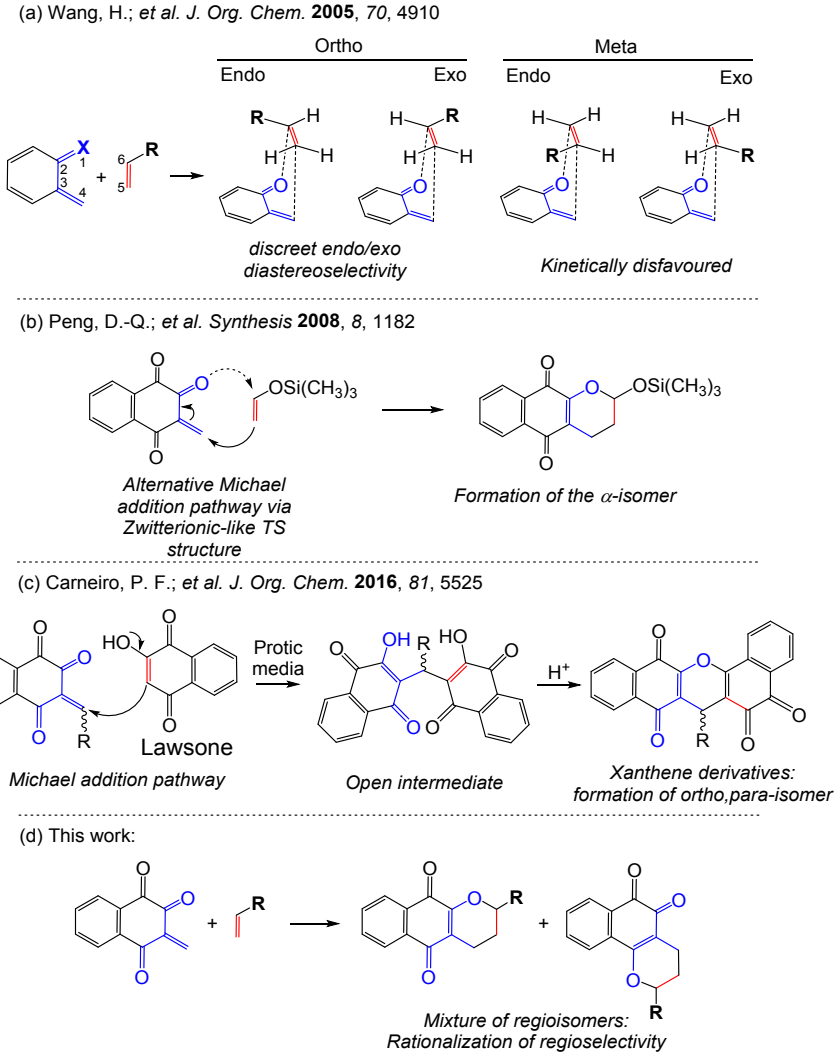

Figure 2. Mechanistic investigation on the regio- and stereoselectivity of the quinone methide intermediate upon hetero-Diels-Alder reactions[12,24,25].

RESULTS AND DISCUSSION

Experimental investigation

The α- and β-lapachone isomers were prepared by an improved methodology recently reported by the current authors[22]: *Ortho* quinone methide was generated *in situ* by the Knoevenagel condensation of lawsone with paraformaldehyde, followed by the hetero-Diels-Alder reaction with different dienophiles in dioxane (**Table 1**).

Table 1. Dienophiles employed in the preparation of α- and β-lapachone derivatives and α:β isomer ratio obtained in each case.

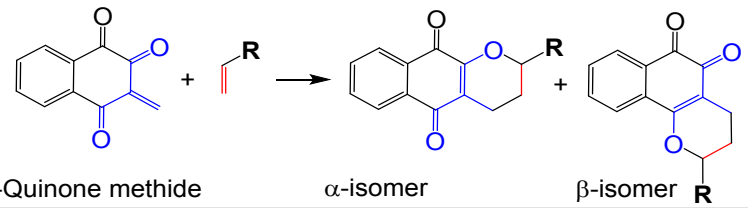

o-Quinone methide α-isomer β-isomer

Entry	Dienophile	Product	α:β (%)	Entry	Dienophile	Product	α:β (%)
1	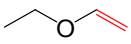	**5**	80:20	7	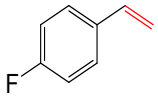	**11**	75:25
2	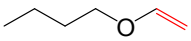	**6**	70:30	8	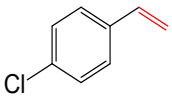	**12**	80:20
3	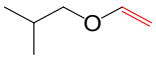	**7**	67:23	9	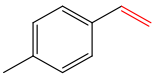	**13**	70:30
4		**8**	88:12	10	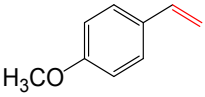	**14**	80:20
5		**9**	75:25	11	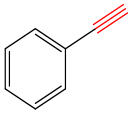	**15**	60:40
6	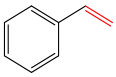	**10**	80:20				

The reaction produced a mixture of α and β isomers in good chemical yields, which was separated on silica gel column chromatography. However, it was only for cyclopentadiene, cyclohexadiene and for the styrene derivatives that was possible to analyze the β isomers by characterization techniques. After separation of the α derivatives from the final product mixture, the β derivatives

of compounds **5**, **6** and **7** were obtained in very small amount and, despite being quantified, their NMR analysis was not possible due to the difficulty of solubility of the material in different deuterated solvents.

The compounds were fully characterized by proton and carbon nuclear magnetic resonance spectroscopy (^{1}H NMR and ^{13}C{1H} NMR, respectively), infrared spectroscopy (IR) and elemental analysis. The ^{1}H NMR spectra show signals between 5.07 – 5.35 ppm for the hydrogen present in the *ortho*- carbon of the chromogenic ring of the β derivatives, which appeared as a double doublet. The aromatic region in the ^{1}H NMR spectrum was used to identify the α- and β-naphthoquinones. The aromatic hydrogens of the β-naphthoquinones split into four signals, while those in the α-naphthoquinones split into only two signals due to the symmetry of the structures. The ^{13}C{1H} NMR spectra also show the formation of the desired products by the signals between 75.0-79.9 ppm due to the differences at carbon 1 of the chromogenic ring. For the reaction with ethynyl benzene as the dienophile, the double bond can be confirmed by the presence of a triplet at 5.68 ppm ($^{3}J_{H,H}$ = 3.6 Hz) in the ^{1}H NMR spectrum (300 MHz, $CDCl_3$), by the highest field shift of the signal of the hydrogens present in the pyran ring (3.35 ppm - $^{3}J_{H,H}$ = 3.6 Hz), as well as by the absence of the signal in the region between 5.00 - 6.00 ppm, corresponding to the hydrogen of the *ortho*- carbon of the chromogenic ring. The quaternary carbon was observed at 100.6 ppm in the ^{13}C-APT NMR spectrum. The *cis*-configuration of the product obtained using cyclopentadiene as dienophile was determined based on the coupling constants between the pyran hydrogens, found in the range of 3.9 Hz.

In order to demonstrate the practical utility of the method as a synthetic tool, the synthesis of products **10a** and **10b** was performed at larger synthetic scale. In this experiment, 28.71 mmols (5 grams) of lawsone and 86.13 mmols (8.97 grams) of styrene were used. 100% conversion was observed and the products **10a** and **10b** were obtained in 75% (3.7 grams) and 25% (1.3 grams) yields, respectively.

For all investigated dienophiles (**Table 1**) it was observed higher selectivity towards the production of the α-isomer with only small variations caused by distinct neighboring groups to the alkenyl moiety. Such interesting feature in the

reactivities of α- and β-moieties within the quinone methide intermediate, although very evident experimentally, represents an unexpected behavior for such species, as both moieties are almost-symmetrical and chemically very similar. In order to rationalize this distinct behavior of α- and β-moieties within the quinone methide intermediate, we further explored these reactions by DFT methods, as will be discussed next.

Regioselectivity in the reactions of dienophiles with the quinone methide intermediate (QM) and related energy barriers

The energy barriers for the hetero-Diels-Alder reaction of $\mathbf{4_H}$ with seven dienophiles (ethene, propene, styrene, methoxyethene, cyclopentadiene and ethynyl benzene), representing those dienophiles that were employed experimentally, were computed. Cyanoethene was also included at this stage of the investigation to complete the set of electron withdrawing groups (EWG) and electron releasing groups (ERG) present in the investigated dienophiles. For each of them, eight approaching modes (reaction channels) of the dienophile over $\mathbf{4_H}$ were considered, with formation of eight distinct transition state structures. Such approaching alternatives are shown in **Figure 3** and the calculated free-energy barriers for their formation are shown in **Figure 4**.

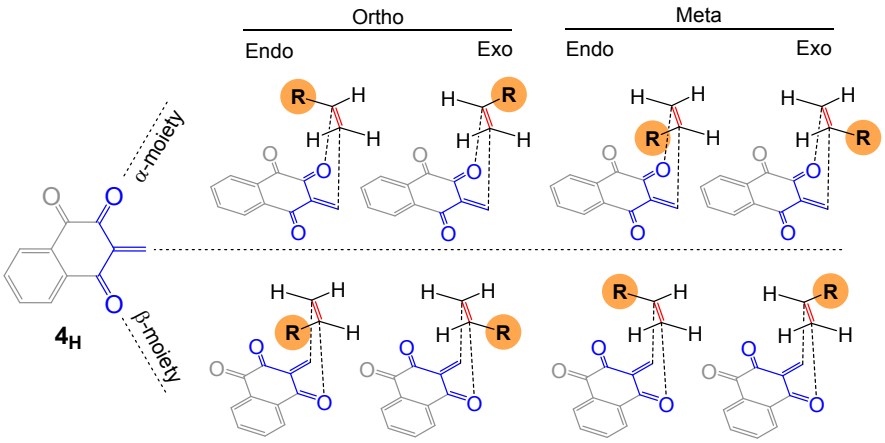

Figure 3. Approaching modes (*ortho*/*meta* and *endo*/*exo*) of the dienophiles over the quinone methide intermediate $\mathbf{4_H}$.

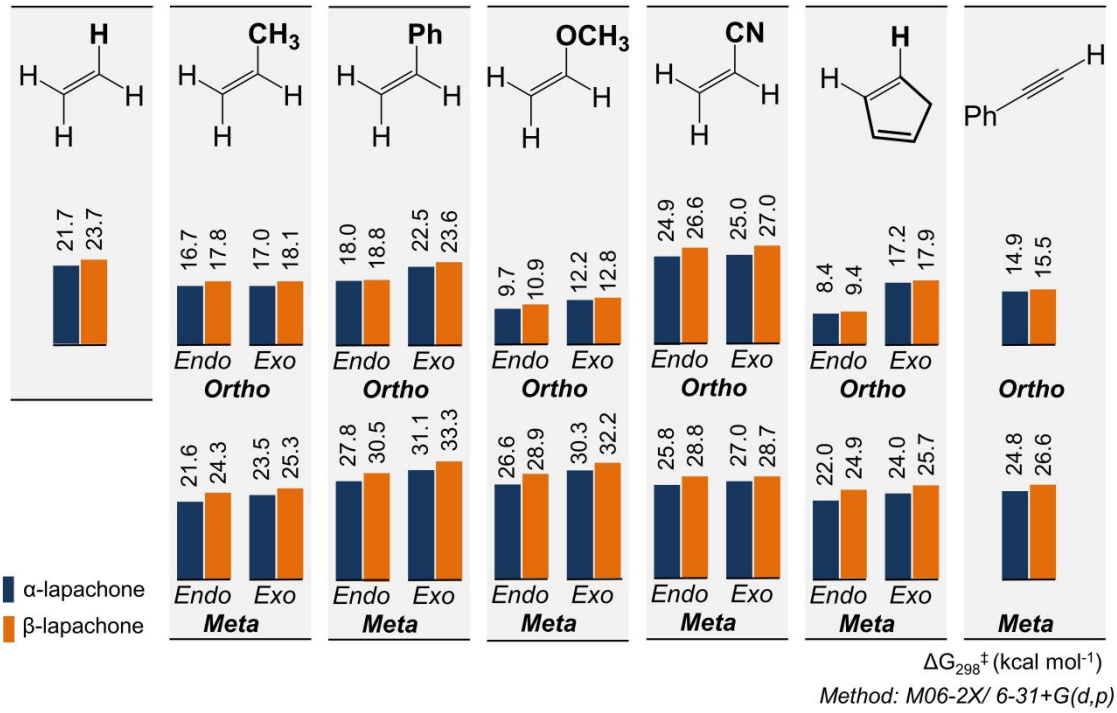

Figure 4. Calculated free-energy barriers for the hetero-Diels-Alder reaction of $\mathbf{4_H}$ and a set of dienophiles (ethene, propene, styrene, methoxyethene, cyanoethene, cyclopentadiene, ethynyl benzene).

In all cases, the lowest energy barriers were obtained for the *ortho-endo* approaching mode, as could be expected from earlier works[24]. We also observed a small *endo*/*exo* diastereoselectivity (energy difference less than 4 kcal mol^{-1}) and *ortho*/*meta* regioselectivity, which is more pronounced for the dienophiles containing an electron releasing group, such as styrene, methoxyethene, cyclopentadiene and ethynyl benzene.

In general, it was observed that regioselectivity is dictated by the *ortho/meta* approach modes of the dienophile to the quinone methide. Electron delocalization in the acrolein-type diene of the quinone methide results in a partial negative charge on the oxygen atom of the acrolein moiety and partial positive charge on the methylene carbon atom. As will be shown below, due to asynchronicity in the formation of the two new bonds, the carbon-carbon bond is formed earlier than the carbon-oxygen bond. This has a direct consequence on the regioselectivity: lower activation energies are expected for orientation of the dienophile´s dipole (when it exists) such that its negative pole is closer to the carbon than to the oxygen atom of the quinone methide (**Figure 5**). This in turn depends on the nature of the substituent group in the dienophile. Electron

releasing groups (ERG) in the dienophile induce a negative pole in the terminal carbon atom (C^1, **Figure 5a**) while electron withdrawing groups (EWG) induce a positive charge in the terminal carbon atom (C^1, **Figure 5b**). These partial charges developed at the carbon atoms C^1 and C^2 of the dienophile result in either larger or smaller energy increase in the transition structure, depending on the chemical identity of the substituent group bonded to C^2. For ERG, *e.g.* -OCH_3, a partial negative charge is developed on C^1, favoring the *ortho* approaching mode (**Figure 5a**), while for EWG, *e.g.* -CN, a partial positive charge is developed on the methylene group C^1 (**Figure 5b**). The relevance of the stabilization of the partial charges developed in the dienophile is illustrated by the cyclopentadiene case. In the orientation shown in **Figure 5c**, the partial positive charge is stabilized by electron delocalization through the vicinal double bond, while in the orientation shown in **Figure 5d** the partial positive charge is isolated from the double bond and undergoes much lower stabilization. The consequence is that only one of the isomers (*ortho*) is observed experimentally. A similar reasoning may be applied to rationalize preferential formation of only one isomer (*ortho*) from the reaction with styrene. The discussion above is centered on the α derivative, but the same may also be applied to the β one.

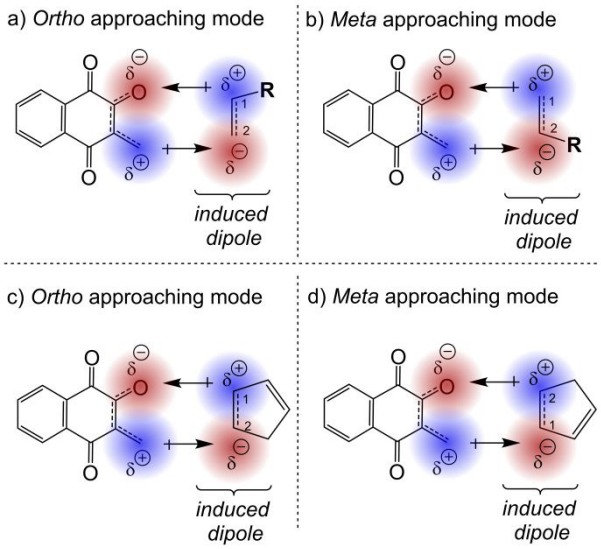

Figure 5. Induced dipole over the dienophiles and the effect of a) electron releasing (ERG) and b) electron withdrawing (EWG) groups in the approach to the diene. c) and d) illustrate the case of cyclopentadiene, favoring the *ortho* approaching mode.

For dienophiles containing an electron withdrawing group, the *meta* approaching mode could be expected as the most stable configuration, however, this is not the case. The carbocationic character developed in the

terminal carbon C^1 (primary carbocation) (**Figure 5b**) results in significant destabilization of the dienophile. Consequently, the energy barriers for the hetero-Diels-Alder reactions in which the dienophile contains an electron withdrawing group are much higher than those computed when R is an electron releasing group. Interestingly, the overall effect is that the *ortho* approaching mode is the preferential one, even for the dienophiles with an electron withdrawing group. In summary, the *ortho* products are the preferential ones for all derivatives, with dienophiles containing an ERG leading to low activation energies, while reactions with dienophiles containing EWG have much higher activation energies.

The reaction with ethynyl benzene apparently undergoes a stepwise mechanism, as we were unable to find a suitable transition state structure with this dienophile corresponding to a concerted cycloaddition process. Our results indicate that the substrate undergoes Michael addition with formation of an open intermediate, which, subsequently, reacts in an intramolecular cycloaddition process to afford the lapachone derivative.

Solvent effect was also taken into consideration for three representative cases: ethene, cyanoethene and methoxyethene (**Tables 2** and **3**). Dioxane was first considered, as it is the experimental solvent used. Water was also considered as solvent, in an attempt to investigate the effect of solvents with higher polarity than dioxane on the transition state structures. In general, we observed that the solvent decreases the activation energies for the hetero-Diels-Alder process, especially when solvent of higher polarity is used, an expected result considering the high polarity of the transition structures. The $\Delta\Delta E^{\ddagger}_{SCF}$ varies from -2.08 to -1.51 kcal mol^{-1} for α-lapachone formation and from -3.20 to -1.75 kcal mol^{-1} for β-lapachone formation.

The concertedness or, conversely, the asynchronicity, was quantified in terms of the Δd parameter (**Table 3**), which is the difference between the C–O and C-C distances in the transition structure[24], with a higher Δd value indicating a higher asynchronicity. Observe that although the oxygen atom is smaller than the carbon atom, the C-C distance in the transition structures for all reactions is smaller than the C-O distance, a clear indication that the C-C bond is formed earlier than the C-O bond. Interestingly, the solvents have a strong effect on the Δd parameter. In all cases, we observed an increase in the Δd parameter when

solvent is taken into account, with the effect increasing in the more polar solvent water. This is consistent with the highly polar character of the transition structures, as discussed before[12,25]. The polar character of the reaction, and consequent asynchronicity, increases when increasing the medium polarity.

Table 2. Solvation effect on the activation energies for the hetero-Diels-Alder reaction of $\mathbf{4_H}$ with ethene, methoxyethene and cyanoethene in the *ortho* approaching mode.

Dienophile	Regioselectivity	Solvent (IEFPCM)	$\Delta E^{\ddagger}_{SCF}$ (kcal mol^{-1})	$\Delta H^{\ddagger}$ (kcal mol^{-1})	$\Delta G^{\ddagger}$ (kcal mol^{-1})
Ethene	α	-	17.93	17.65	21.75
		Dioxane	17.18	16.89	20.86
		Water	15.85	15.62	19.42
	β	-	19.87	19.60	23.68
		Dioxane	18.85	18.58	22.64
		Water	17.08	16.85	20.53
Cyanoethene	α	-	21.09	20.71	24.87
		Dioxane	20.53	20.09	23.97
		Water	19.58	19.27	24.10
	β	-	23.19	22.77	26.57
		Dioxane	22.47	22.08	25.88
		Water	21.44	21.24	26.14
Methoxyethene	α	-	5.71	5.74	9.70
		Dioxane	4.90	4.94	8.90
		Water	4.07	3.77	6.40
	β	-	7.30	7.14	10.86
		Dioxane	5.78	5.64	9.02
		Water	4.10	3.83	6.70

The experimental α/β regioselectivity observed for the reaction with $\mathbf{4_H}$ is also nicely reproduced by our theoretical calculations. For all reactions computed, the transition state structure for formation of α-lapachone has lower energy than the corresponding one for formation of β-lapachone. This occurs for all considered reaction pathways and in the formation of all considered regio- and diastereoisomers, even including the implicit solvation effect. The reason for preferential formation of the α isomer is not so obvious[22]. In trying to find a rationalization for this preference, we decided to explore in detail the energy profile for the reaction of $\mathbf{4_H}$ with ethene.

Table 3. Interatomic distances of $C_{dienophile}$-C_{diene} and $C_{dienophile}$-O_{diene} obtained in the optimized transition state structures and asynchronicity measurement (Δd).

			Interatomic distances (Å)		
Dienophile	isomer	Solvent effect	$C_{dienophile}$-C_{diene}	$C_{dienophile}$-O_{diene}	Δd (Å)
Ethene	α	Gas phase	2.027	2.293	0.266
		Dioxane[a]	2.009	2.343	0.334
		Water[a]	1.984	2.435	0.448
	β	Gas phase	1.970	2.302	0.333
		Dioxane[a]	1.956	2.356	0.400
		Water[a]	1.941	2.455	0.514
Propene	α	Gas phase	1.945	2.498	0.553
	β	Gas phase	1.864	2.556	0.692
Styrene	α	Gas phase	1.907	2.823	0.916
	β	Gas phase	1.860	2.941	1.081
Methoxyethene	α	Gas phase	2.090	2.792	0.720
		Dioxane[a]	2.146	2.889	0.743
		Water[a]	2.233	3.013	0.780
	β	Gas phase	2.033	2.856	0.823
		Dioxane[a]	2.100	2.966	0.866
		Water[a]	2.223	3.047	0.824
Cyanoethene	α	Gas phase	1.932	2.269	0.337
		Dioxane[a]	1.927	2.286	0.359
		Water[a]	1.920	2.312	0.392
	β	Gas phase	1.901	2.273	0.372
		Dioxane[a]	1.897	2.288	0.391
		Water[a]	1.883	2.318	0.435
Cyclopentadiene	α	Gas phase	2.052	2.865	0.813
	β	Gas phase	2.044	2.906	0.862
Ethynylbenzene	α	Gas phase	1.864	-[b]	-
	β	Gas phase	1.844	-[b]	-

[a]IEFPCM solvation model; [b]Formation of Michael addition intermediate.

*The reaction between **4_H** and ethene along a generic reaction coordinate*

The origin of the α/β-regioselectivity observed for the hetero-Diels-Alder reactions between **4_H** and ethene was investigated by analysis of the Potential Energy Surfaces (PES) leading from the pre-reactive complexes (**IC**) to the transition structures (**$TS_α$** and **$TS_β$**, respectively) for both reactions. We computed a set of points along the IRC going from the transition structure to the pre-reactive complex and analyzed them according to the Activation Strain Model (ASM) and the Energy Decomposition Analysis (EDA). For the purpose of comparing equivalent points along both (α and β) reaction coordinates, we had to develop an alternative description of the progress of the reaction as it progresses from the pre-reactive complex to the transition structure.

Based on the Activation Strain Model (ASM), we wanted to quantify the deformation in the geometry as the reaction advanced from the reactants to the transition structure. Observe that the reorganization energy, which has been

usually taken as a measurement of the reaction coordinate, is not suitable in the present case, as it is not possible to define a unique and simultaneous reorganization energy for both reactions, leading either to the α- or the β derivatives. The starting point was then to define a new generic reaction coordinate that could take into account the most relevant structural changes occurring in both, the dienophile and in the quinone methide and that could be measured in equivalent positions for both reactions. Therefore, we defined a new reaction coordinate, $\mathbf{q_{sz}}$, which is computed considering two components: contributions from deformations in dihedral angles and in bond lengths. From these we took the most relevant ones, *i.e.* the six lengths of changing/forming bonds involved in the cycloaddition reaction and the C-C-H(H) dihedral angles of the three methylene groups - two methylene groups of ethene and the methylene group of $\mathbf{4_H}$ (**Figure 6a**). The weight of each of these components to the final value of $\mathbf{q_{sz}}$ was determined by the contribution of each of them to the overall reorganization energy along the **IC** → $\mathbf{TS_\alpha}$ process, according to the Activation Strain Model (**Figure 6b**). We observed that roughly 70% of the reorganization energy (13.2 kcal mol^{-1} in a total of 19.4 kcal mol^{-1}) is due to the distortion of the dihedral angles and that distortion of the bond length contributed to circa 30% (6.18 kcal mol^{-1}).

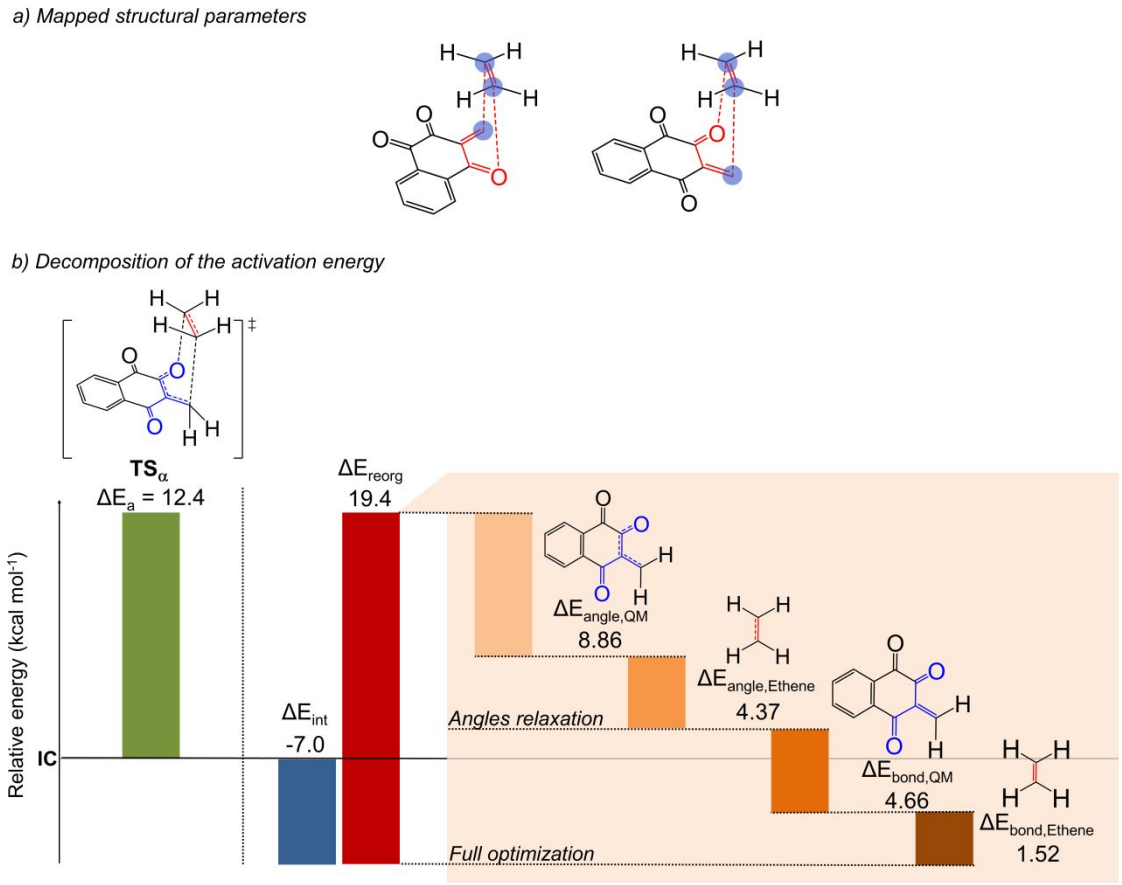

Figure 6. Illustration of the mapped structural parameters for the definition of the reaction coordinate $\mathbf{q_{sz}}$ (a): six lengths of changing/forming bonds involved in the cycloaddition reaction (red lines) and the C-C-H(H) dihedral angles of the three methylene groups (blue circles). Decomposition of the activation energy into interaction and reorganization energy and contributions of dihedral angles and bond lengths deformation for the reorganization energy (b).

The changes in bond lengths and dihedral angles were mapped and the corresponding **s** and **z** reaction coordinate components (Equations 1 and 2) were calculated for each point obtained along the IRC curve. In Equation 1, ***dR*** and ***dP*** correspond to the individual bond lengths mapped in the pre-reactive complex and final product, respectively, whereas ***di*** corresponds to the individual bond lengths mapped in each point of the IRC curve. Similarly, ***ai***, ***aR***, and ***aP*** correspond to the dihedral angles mapped in each point of the IRC curve, in the pre-reactive complex, and in the final product.

Next, the **s** and **z** parameters for the reaction forming the α derivative were normalized against the range of values between the pre-reactive complex (**IC**) and the transition structure ($\mathbf{TS_\beta}$) for the reaction forming the β derivative, the one with the highest reorganization energy. The normalization was done using Equations 3 and 4, in which $\mathbf{s_{100}}$ and $\mathbf{z_{100}}$ are the normalized parameters, **s** and

z are the parameters calculated by Equations 1 and 2 for each point along the IRC curve, and **s(TS_β)** and **z(TS_β)** are the corresponding parameters calculated for the transition structure **TS_β**. According to Equations 1 and 2, **s(TS_β)** and **z(TS_β)** are equal to 0.706 and 0.200, respectively.

When taken together, and considering the weights determined previously, we quantified the generic reaction coordinate $\mathbf{q_{sz}}$ according to Equation 5. In Equation 5, $\mathbf{s_{100}}$ and $\mathbf{z_{100}}$ are those obtained from Equations 3 and 4, respectively. It is important to mention that the pre-reactive complex (**IC)** considered here has adequate symmetry and orientation for following both reaction paths, being therefore an equivalent initial point for both reactions.

$$\mathbf{s} = \frac{\sum|\boldsymbol{di} - \boldsymbol{dR}|}{\sum|\boldsymbol{dP} - \boldsymbol{dR}|} \text{ (Equation 1)}$$

$$\mathbf{z} = \frac{\sum|\boldsymbol{ai} - \boldsymbol{aR}|}{\sum|\boldsymbol{aP} - \boldsymbol{aR}|} \text{ (Equation 2)}$$

$$\mathbf{s_{100}} = \frac{\mathbf{s}}{\mathbf{s}(\mathbf{TS_\beta})} \text{ (Equation 3)}$$

$$\mathbf{z_{100}} = \frac{\mathbf{z}}{\mathbf{z}(\mathbf{TS_\beta})} \text{ (Equation 4)}$$

$$\mathbf{q_{sz}} = \mathbf{0.3} \times \mathbf{s_{100}} + \mathbf{0.7} \times \mathbf{z_{100}} \text{ (Equation 5)}$$

For the plots in **Figure 7** it is necessary to associate the $\mathbf{q_{sz}}$ reaction coordinate with labels that identifies the points along the reaction coordinate and the α- or β-lapachone PES. For this, we use $\mathbf{q_{sz}}$(x,y), where $\mathbf{q_{sz}}$ represents the reaction progress and is the value plotted in the abscissa of the energy profiles, x labels the key points along the reaction coordinate (usually indicating **TS_α** or **TS_β**) and y indicates the referred PES as belonging to α- or β-lapachone (α or β, respectively). For instance, the $\mathbf{q_{sz}}$ point corresponding to the transition state of α-lapachone is written as $\mathbf{q_{sz}}$(**TS_α**,α); the transition state of β-lapachone is written as $\mathbf{q_{sz}}$(TS_β,β); and the point on the PES of β-lapachone that corresponds to the transition state of α-lapachone is written as $\mathbf{q_{sz}}$(**TS_α**,β).

Following the PES for β-lapachone in **Figure 7(a)**, **TS_β** is located at $\mathbf{q_{sz}}$(**TS_β**,β) = 1 (as defined by our normalization process), whereas following the PES for α-lapachone, **TS_α** is located at $\mathbf{q_{sz}}$(**TS_α**,α) = 0.95. Following this

procedure, we found the point on the β-lapachone PES corresponding to $\mathbf{TS_\alpha}$ $\mathbf{q_{sz}}(\mathbf{TS_\alpha},\beta) = 0.95$. Therefore, when taken on the same basis, the transition state of β-lapachone ($\mathbf{TS_\beta}$, $\mathbf{q_{sz}}(\mathbf{TS_\beta},\beta) = 1.00$) is, indeed, more lately formed than $\mathbf{TS_\alpha}$, in connection with the Hammond postulate[26]. Having defined equivalent reaction coordinates for both PES, the points $\mathbf{q_{sz}}(\mathbf{TS_\alpha},\beta)$ can now be compared to $\mathbf{q_{sz}}(\mathbf{TS_\alpha},\alpha)$ and the Activation Strain Model (ASM) and Energy Decomposition Analysis (EDA) can be used to rationalize and identify the origin of the lateness of $\mathbf{TS_\beta}$.

At $\mathbf{q_{sz}}(\mathbf{TS_\alpha},\alpha)$ and $\mathbf{q_{sz}}(\mathbf{TS_\alpha},\beta)$, the computed reorganization energy (E_{Reorg}) is roughly identical in both cases (**Figure 7(a)**), varying only by 0.4 kcal mol^{-1}. This is quite reasonable, as according to our reaction coordinate model, at $\mathbf{q_{sz}}(TS_\alpha,\alpha)$ and $\mathbf{q_{sz}}(TS_\alpha,\beta)$ the reaction progress and the distortion of the reactants for formation of the α- and β-derivatives should be identical. On the other hand, the interaction energy (E_{Int}) is significantly different for $\mathbf{q_{sz}}(TS_\alpha,\alpha)$ and $\mathbf{q_{sz}}(TS_\alpha,\beta)$, reaching -7.0 kcal mol^{-1} at $\mathbf{q_{sz}}(TS_\alpha,\alpha)$, but only -4.8 kcal mol^{-1} at $\mathbf{q_{sz}}(TS_\alpha,\beta)$.

It is interesting to notice that if equivalent points on both PES were not considered, but instead the two transition state structures were directly compared, the energy barrier difference for both reactions would be erroneously attributed to the distortion energy for forming these transition states: $E_{Reorg}(\mathbf{TS_\alpha})$ = 19.4 kcal mol^{-1} and $E_{Reorg}(\mathbf{TS_\beta})$ = 21.6 kcal mol^{-1}. However, as it will be shown next, this is the result of distinct interaction energies acting at each point of both PES. The reorganization energy curves for both reactions **Figure 7(a)** present very small energy differences, which become quite evident when E_{Reorg} is computed at $\mathbf{q_{sz}}(TS_\alpha,\alpha)$ and $\mathbf{q_{sz}}(TS_\alpha,\beta)$, 19.4 and 19.0 kcal mol^{-1}, respectively.

The Energy Decomposition Analysis (EDA) was additionally used to decompose the computed interaction energies at $\mathbf{q_{sz}}(\mathbf{TS_\alpha},\alpha)$ and $\mathbf{q_{sz}}(\mathbf{TS_\alpha},\beta)$ into electrostatic, Pauli repulsion, polarization, exchange and dispersion energy terms (E_{ES}, E_{REP}, E_{POL}, E_{EX} and E_{DISP}, respectively). As shown in **Figure 7(b)**, the dispersion energy term is roughly identical at these points (ΔE_{DISP} = -0.24 kcal mol^{-1}). Electrostatic, polarization and exchange energy terms present more negative values for $\mathbf{q_{sz}}(\mathbf{TS_\alpha},\beta)$ (ΔE_{ES} = -1.94 kcal mol^{-1}, ΔE_{POL} = -1.36 kcal mol^{-1} and ΔE_{EX} = -3.18 kcal mol^{-1}). Finally, the Pauli repulsion term is much more destabilizing at $\mathbf{q_{sz}}(\mathbf{TS_\alpha},\beta)$ than at $\mathbf{q_{sz}}(\mathbf{TS_\alpha},\alpha)$ (ΔE_{REP} = +8.92 kcal mol^{-1}) and the

overall effect is the observed lower interaction energy at $\mathbf{q_{sz}}(\mathbf{TS_\alpha},\beta)$ than at $\mathbf{q_{sz}}(\mathbf{TS_\alpha},\alpha)$, ΔE_{Int} being equal to +2.19 kcal mol^{-1}. The higher increase of the Pauli repulsion term on the β PES results that $\mathbf{TS_\beta}$ is achieved in a later stage than $\mathbf{TS_\alpha}$, where the stabilizing terms (dispersion, electrostatic, polarization and exchange energies) are able to overcome the destabilizing Pauli repulsion term.

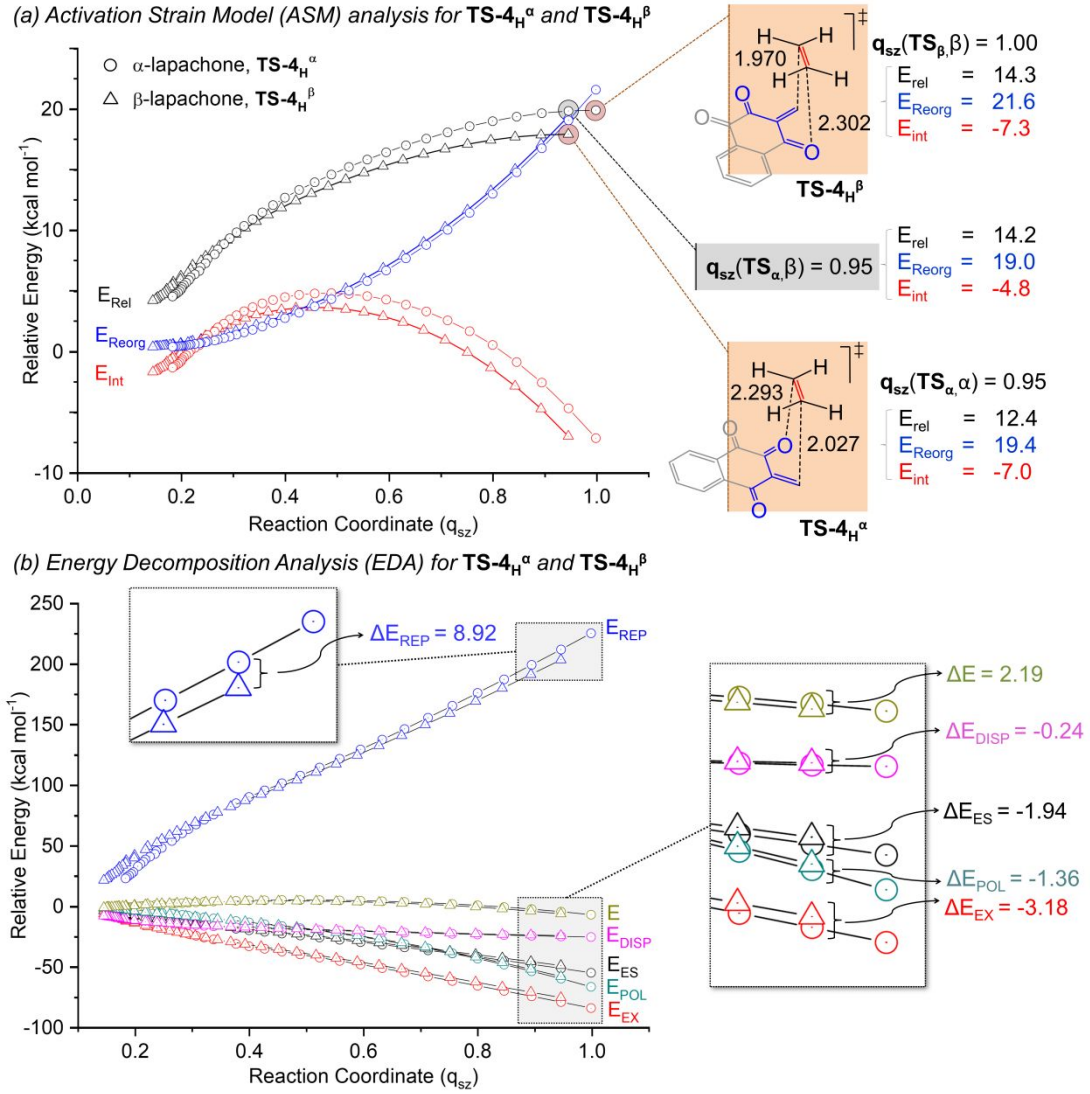

Figure 7. Activation Strain Model (ASM) and Energy Decomposition Analysis (EDA) of all IRC points obtained from $\mathbf{TS_\alpha}$ and $\mathbf{TS_\beta}$ towards the initial complex. The abscissa describes the advances of the reaction according to the $\mathbf{q_{sz}}$ coordinate.

Within the EDA scheme for the decomposition of the interaction energy between two fragments, the Pauli repulsion term (E_{REP}) accounts for energy increase necessary for going from the superposition of the unperturbed electron

density of the separated fragments to the antisymmetrized and renormalized individual wavefunctions of the fragments before Kohn-Sham orbital relaxation[27,28]. This term has been frequently associated with the repulsion between closed shell orbitals and is an indicator of the steric repulsion between the fragments[27,28]. For the hetero-Diels-Alder reaction investigated here, however, the repulsion between the closed shell sp^2 orbitals within the quinone methide fragment $\mathbf{4_H}$ may be the major source for the E_{REP} differences observed for the α- and β-lapachone PES.

The destabilizing interaction between sp^2 orbitals of neighboring carbonyl groups in the 1,2-quinone derivatives is clearly seen when their energy is compared to their 1,4-isomer (**Table 4**). Considering three common quinones isomer pairs (1,2-/1,4-quinone, 1,2-/1,4-naphtoquinone and 2-/4-lawsone), as well as α-/β-lapachone, we always find the 1,4 (or α-derivative) as the most stable species (**Table 4**). In trying to find a connection between the relative stability of these species and their structure we broken each of them into their respective triplet acrolein diradicals, as shown by the dashed lines over each structure of **Figure 3**. The interaction energy (E_{int}) between the two fragments were then computed.

Table 4. Relative energy difference for bringing together the corresponding triplet acrolein diradicals shown below (separated by dashed lines) for formation of 1,2-/1,4-quinone, 1,2-/1,4-naphtoquinone, 2-/4-lawsone and α-/β-lapachone.

	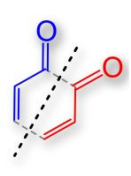	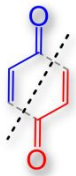	**ΔE**	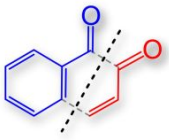	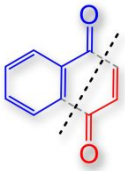	**ΔE**
$\mathbf{E_{SCF,Relative}}$	7.23	0.00	-	7.40	0.00	-
$\mathbf{E_{int}}$	-202.90	-209.40	-6.50	-204.75	-212.12	-7.38
	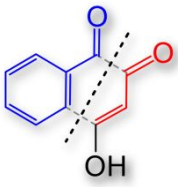	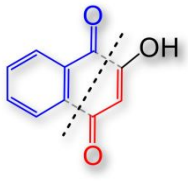	**ΔE**	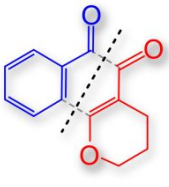	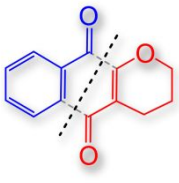	**ΔE**
$\mathbf{E_{SCF,Relative}}$	3.89	0.00	-	4.44	0.00	-
$\mathbf{E_{int}}$	-205.18	-208.62	-3.34	-203.94	-208.32	-4.38

Method: M06-2X/6-31+G(d,p)

A direct correlation between the relative stability of these isomers and the interaction energy between the acrolein diradicals can be observed. Additionally, for lawsone and lapachone, the relative energy between isomers, as well as the interaction energy difference between the radicals, decrease significantly when compared to 1,2-/1,4-quinone and 1,2-/1,4-naphtoquinone. This is a direct effect of the additional oxygen atom bonded to the quinone core, which results in a smaller relief of the electronic repulsion between sp^2 orbitals when going from 4-lawsone to 2-lawsone or from β-lapachone to α-lapachone.

The same repulsion can be expected within $\mathbf{4_H}$ between C^1=O and C^2=O, which must decrease as the reaction proceeds towards the formation of $\mathbf{TS_\alpha}$ and the rehybridization of the oxygen at C^2 takes place. For formation of $\mathbf{TS_\beta}$, on the other hand, such electronic repulsion remains throughout the reaction path, resulting in the steepest increase of the E_{REP} curve observed in **Figure 7**.

Overall, these results show that the α-selectivity of the hetero-Diels-Alder reactions involving the quinone methide $\mathbf{4_H}$ is due to the Pauli repulsion of its C^1=O and C^2=O carbonyl groups and consequent higher reactivity of the α-moiety when compared to the β-moiety towards the relaxation of such destabilizing interaction.

CONCLUSIONS

The hetero-Diels-Alder reaction between 3-methylene-1,2,4-naphthotriones ($\mathbf{4_H}$) and a set of dienophiles (ethene, propene, styrene, methoxyethene, cyanoethene, cyclopentadiene and ethynyl benzene) has been investigated. Throughout this investigation, *endo*/*exo*, *ortho*/*meta* and α/β selectivity was taken into account considering eight approaching modes of the dienophiles over $\mathbf{4_H}$. Discreet *endo*/*exo* diastereoselectivity was computed for these reactions ($\Delta\Delta G^{\ddagger}$ < 4 kcal mol^{-1}) and pronounced *ortho*/*meta* regioselectivity for dienophile containing an electron releasing groups, achieving $\Delta\Delta G^{\ddagger}$ of circa 19 kcal mol^{-1}. In all cases, the lowest energy barriers were computed for the *ortho*-*endo* approaching mode.

Solvent effect over the hetero-Diels-Alder process was also take into consideration, revealing a decrease of the energy barriers, with $\Delta E^{\ddagger}_{SCF}$ varying from - 2.08 to -1.51 kcal mol^{-1} for α-lapachone formation and from -3.20 to -1.75

kcal mol^{-1} for β-lapachone formation. The concertedness of the transition state structure for the hetero-Diels-Alder reaction was also observed to decrease, with the asynchronicity measurement (Δd) increasing significantly with the polarity of the solvent.

The experimentally observed α-selectivity was thoroughly investigated by means of the Activation Strain Model (ASM) and Energy Decomposition Analysis (EDA) approaches. Comparison of equivalent points on α- and β-lapachone Potential Energy Surfaces revealed that lower Pauli Repulsion is observed over the reaction path for formation of α-lapachone when compared to β-lapachone. The reduction of repulsive interaction between sp^2-like orbitals of C^1=O and C^2=O groups within $\mathbf{4_H}$ during the formation of $\mathbf{TS_\alpha}$ is considered to be the major origin for this effect. For reaction forming the β derivatives the C^1=O and C^2=O groups remain unaltered and therefore there is no release on the steric interaction.

EXPERIMENTAL SECTION

Experimental details.

Analytical grade solvents were used. Reagents were purchased from Aldrich or Acros Chemical Co. Column chromatography was performed on silica gel 60 (Merck 70-230 mesh). Yields refer to chromatographically and spectroscopically homogeneous materials. Reactions were monitored by thin-layer chromatography (TLC) carried out on 0.25 mm E. Merck silica gel plates (60F-254) using UV light as visualizing agent and/or with ethanol solution of 3% vanillin in sulfuric acid followed by heating. Infrared spectra were recorded on a Perkin-Elmer FT-IR Spectrum One spectrophotometer, calibrated relative to the 1601.8 cm^{-1} absorbance of polystyrene; values are reported in cm^{-1}. Melting points were observed on a Fischer-Johns melting point apparatus. NMR spectra were recorded on a Varian Unity Plus VXR (300 MHz) equipment in DMSO-d_6 or $CDCl_3$ solutions and tetramethylsilane as the internal standard (δ = 0 ppm). In case of multiplets, the signals were reported as intervals. Signals were abbreviated as s, singlet; d, doublet; t, triplet; m, multiplet. High-resolution mass spectra (HRMS) were recorded on an MICROMASS Q-TOF MICRO Mass spectrometer using ESI-TOF (electrospray ionization-time of flight). Purity of

final compounds was established using elemental analysis. All compounds were ascertained based on their elemental analysis.

General Procedure for preparation of pyran naphthoquinones. To a round-bottom flask equipped with a magnetic stirring bar, lawsone was dissolved (1 mmol) in dioxane (20 mL), followed by addition of formaldehyde (8 mmol). The dienophile (3 mmol) was added dropwise and the reaction mixture was stirred under reflux until consumption of the starting material. The solvent was removed under reduced pressure; ethyl acetate was added in the residue and the mixture was washed with saturated sodium bicarbonate aqueous solution. The combined organic extract was washed with water, dried over anhydrous sodium sulfate, filtered and concentrated under vacuum. The residual mixture of products was purified by flash chromatography employing gradient *n*-hexane/EtOAc as eluent, furnishing the desired 1,2 and 1,4-naphthoquinones.

2-ethoxy-3,4-dihydro-2H-benzo[g]chromene-5,10-dione (5).[29] Compound **5** was obtained as a yellow solid in 80% yield (140 mg). m.p.= 168-170 ^{0}C; IR (film, $CHCl_3$) ν(cm^{-1}): 3418, 2929, 1713, 1595, 1269, 1251, 1014, 941, 736; ^{1}H NMR ($CDCl_3$, 300 MHz): δ 1.19 (3H, t, *J* = 7.0 Hz, C$\underline{H}_3$), 1.79-1.90 (2H, m, H-4), 2.12 (2H, t, *J* = 2.4 Hz, H-3), 5.47 (1H, t, *J* = 2.4 Hz, H-2), 3.72 (1H, ddd, *J* = 4.3, 7.0 and 9.7 Hz, OC$\underline{H}_2$), 3.92 (1H, ddd, *J* = 4.3, 7.0 and 9.7 Hz, OC$\underline{H}_2$), 7.68 (2H, dddd, *J* = 1.7, 7.3, 9.2 and 11.0 Hz, H-8 and H-7), 8.08 (2H, dddd, *J* = 1.7, 7.3, 9.2 and 11.0 Hz, H-9 and H-6); ^{13}C{1H} NMR ($CDCl_3$, 75 MHz): δ 14.5 (C$\underline{H}_3$), 15.2 (C$\underline{H}_2$), 25.2 (C$\underline{H}_2$), 65.0 (OC$\underline{H}_2$CH$_3$), 98.4 (C-2), 122.9 (C-4a), 126.3, 126.4, 133.2 and 134.1 (C-Har), 131.2 (C-9a), 132.1 (C-5a), 152.8 (C-10a), 184.4 (C=O). HRMS (ESI/Q-TOF) m/z: [M + Na]$^+$ Calcd for $C_{15}H_{14}O_4Na$ 281.0892; Found 281.0886. Anal. Calcd for $C_{15}H_{14}O_4$: C, 69.76; H, 5.46. Found: C, 69.73; H, 5.40.

2-butoxy-3,4-dihydro-2H-benzo [g]chromene-5,10-dione (6).[29] Compound **6** was obtained as a yellow solid in 70% yield (120 mg). M.p.= 168-170 ^{0}C; IR (film, $CHCl_3$) ν(cm^{-1}):3436, 2924, 2854, 1770,1713, 1596, 1280, 1064, 940, 723; ^{1}H NMR ($CDCl_3$, 300 MHz): δ 0.86 (3H, t, *J* = 7.3 Hz, CH_3); 1.25-1.38 (1H, m, CH_2); 1.50-1.60 (1H, m, CH_2); 1.79-1.90 (2H, m, CH_2); 2.09-2.17 (2H, m, CH_2); 3.65 (1H, ddd, *J* = 3.1; 6.5 and 9.7 Hz, OCH_2); 3.88 (1H, ddd, *J* = 3.1; 6.5 and

9.7 Hz, OCH_2); 5.47 (1H, t, *J* = 2.6 Hz, H-2); 7.70 (2H, dddd, *J* = 1.7; 7.3; 9.2; 11.0 Hz, H-8 and H-7); 8.09 (2H, dddd, *J* = 1.7; 7.3; 9.0; 10.9 Hz, H-9 and H-6); $^{13}C\{1H\}$ NMR ($CDCl_3$, 75 MHz): δ 14.1 (CH_3); 13.5 (CH_2CH_3); 18.9 (C-4); 24.8 (C-3); 31.3 ($CH_2CH_2CH_3$); 68.9 (OCH_2CH_3); 98.2 (C-2); 122.5 (C-4a); 125.9; 126.0; 130.8 and 132.8 (C-Har); 131.7 (C-9a); 133.7 (C-5a); 152.2 (C-10a); 184.0 (C=O). HRMS (ESI/Q-TOF) m/z: $[M + Na]^+$ Calcd for $C_{17}H_{18}O_4Na$ 309.1205; Found 309.1210. Anal. Calcd for $C_{17}H_{18}O_4$: C, 71.31; H, 6.34. Found: C, 71.20; H, 6.40.

2-isobutoxy-3,4-dihydro-2H-benzo[g]chromene-5,10-dione (7). Compound **7** was obtained as a yellow solid in 67% yield (117 mg). M.p.= 145-148 ^0C; IR (film, $CHCl_3$) ν(cm^{-1}): 3340, 2957, 1678, 1651, 1387, 1301, 1259, 957, 720; ^1H NMR ($CDCl_3$, 300 MHz): δ 0.85 (6H, t, *J* = 6.7 Hz, $2CH_3$), 1.79-1.91 (2H, m, H-3), 2.15 (1H, t, *J* = 6.7 Hz, $CH(CH_3)_2$), 2.53-2.76 (2H, m, H-4), 3.43 (1H, dd, *J* = 6.7 and 9,5 Hz, OCH_2), 3.66 (1H, dd, *J* = 6.7 and 9.5 Hz, OCH_2), 5.46 (1H, t, *J* = 2.5 Hz, H-2), 7.69 (2H, dddd, *J* = 1.8, 7.5, 9.2 and 10.9 Hz, H-8 and H-7), 8.09 (2H, dddd, *J* = 1.8, 7.5, 9.2 and 10.9 Hz, H-9 and H-6); $^{13}C\{1H\}$ NMR ($CDCl_3$, 75 MHz): δ 14.1 (C-4), 18.9 (CH_3), 24.8 (C-3), 28.2 ($CH(CH_3)_2$), 75.6 ($OCH_2CH(CH_3)_2$), 98.2 (C-2), 122.6 (C-4a), 125.8, 126.0, 132.8 and 133.7 (C-Har), 130.8 (C-9a), 131.7 (C-5a), 152.5 (C-10a), 184.0 (C=O); HRMS (ESI/Q-TOF) m/z: $[M + Na]^+$ Calcd for $C_{17}H_{18}O_4Na$ 309.1205; Found 309.1215. Anal. Calcd for $C_{17}H_{18}O_4$: C, 71.31; H, 6.34. Found: C, 71.40; H, 6.38.

(±)-11,11a-dihydrobenzo[g]cyclopenta[b]chromene-5,10(1H,3aH)-dione (8a). [29] Compound **8a** was obtained as a yellow solid in 88% yield (153 mg). M.p.= 140-142 ^0C; IR (film, $CHCl_3$) ν(cm^{-1}): 2885, 2851, 1676, 1643, 1386, 1198, 1011, 932, 725; ^1H NMR ($CDCl_3$, 300 MHz): δ 2.30-2.29 (1H, m, H-4a), 2.50-2.62 (3H, m, H-4 and H-5), 2.97-2.89 (1H, m, H-5), 5.32 (1H, d, *J* = 2.6 Hz, H-1a), 6.11-6.15 (1H, m, H-3), 6.23-6.27 (1H, m, H-2), 7.85-7.94 (2H, m, H-9 and H-8), 8.04-8.08 (2H, m, H-10 and H-7); $^{13}C\{1H\}$ NMR ($CDCl_3$, 75 MHz): δ 19.7 (C-4), 34.0 (C-4a), 37.5 (C-5), 83.2 (C-1a), 119.7 (C-5a), 125.6, 125.9, 130.9 and 137.0 (C-Har), 130.6 (C-6a), 131.6 (C-10a), 133.5 (C-2 or C-3), 134.3 (C-2 or C-3), 155.8 (C-11a), 178.8 and 183.5 (C=O); HRMS (ESI/Q-TOF) m/z: $[M + Na]^+$ Calcd for $C_{16}H_{12}O_3Na$ 275.0786; Found 275.0795. Anal. Calcd for $C_{16}H_{12}O_3$: C, 76.18; H, 4.79. Found: C, 76.09; H, 4.73.

(±)-7a,8-Dihydrobenzo[h]cyclopenta[b]chromene-5,6(7H,10aH)-dione (8b).[11] Compound **8b** was obtained as a orange solid in (21mg) 12% yield. M.p.= 146-147 ^{0}C; IR (film, $CHCl_3$) ν(cm^{-1}): 2975, 2931, 1738,1716, 1599, 1284, 959, 927, 720; ^{1}H NMR (DMSO-d6, 300 MHz): δ 2.23-2.32 (1H, m, H-5), 2.47-2.54 (1H, m, H-5), 2.66-2.95 (3H, m, H-4 and H-4a), 5.48-5.50 (1H, m, H-1a), 6.28-6.31 (1H, m H-3), 6.18-6.21 (1H, m H-2), 7.68 – 7.73 (1H, m, ArH), 7.85-7.87 (2H, m, ArH), 8.01-8.08 (1H, m, ArH); ^{13}C{1H} NMR (DMSO-d6, 75 MHz): δ 19.7 (C-5), 34.5 (C-4a), 37.9 (C-4), 85.0 (C-1a), 112.5 (C-5a), 124.4 (C-3), 135.7 (C-2), 128.5, 131.2, 131.5 and 135.7 (C-ar), 130.3 (C-7a), 132.6 (C-11a), 163.6 (C-11b), 178.4 and 179.8 (2C=O); HRMS (ESI/Q-TOF) m/z: $[M + Na]^+$ Calcd for $C_{16}H_{12}O_3Na$ 275.0786; Found 275.0785. Anal. Calcd for $C_{16}H_{12}O_3$: C, 76.18; H, 4.79. Found: C, 76.10; H, 4.76.

(±)-3,4,4a,5-tetrahydrobenzo[g]pyrano[2,3-b]chromene-6,11(2H,12aH)-dione (9a).[29] Compound **9a** was obtained as a yellow solid in 75% yield (130 mg). M.p.= 163-165 ^{0}C; IR (film, $CHCl_3$) ν(cm^{-1}): 2936, 1678, 1645, 1623, 1348, 1194, 1145, 954, 721; ^{1}H NMR ($CDCl_3$, 300 MHz): δ 1.53-1.64 (2H, m, H-6), 1.71-1.79 (2H, m, H-4), 2.19-2.29 (1H, m, H-5), 2.65 (1H, d, *J* = 2.5, H-5a), 3.74-3.81 (1H, m H-3), 3.97-4.05 (1H, m H-3), 5.44 (1H, d, *J* = 2.5, H-1a), 7.67-7.73 (2H, m, H-10 and H-9), 8.05 (2H, m, H-11 and H-8); ^{13}C{1H} NMR ($CDCl_3$, 75 MHz): δ 23.4 (C-4), 23.7 (C-5 and C-6), 30.3 (C-5a), 62.5 (C-3), 97.9 (C-1a), 119.4 (C-6a), 125.8, 126.1, 132.9 and 133.7 (C-Har), 130.8 (C-7a), 131.7 (C-11a), 153.0 (C-12a), 184.1 (2C=O); HRMS (ESI/Q-TOF) m/z: $[M + Na]^+$ Calcd for $C_{17}H_{14}O_3Na$ 289.0943; Found 289.0930. Anal. Calcd for $C_{17}H_{14}O_3$: C, 76.68; H, 5.30. Found: C, 76.65; H, 5.28.

(±)-7,7a,8,9-Tetrahydro-5H-benzo[c]xanthene-5,6(11aH)-dione (9b).[11] Compound **9b** was obtained as a orange solid in (44mg) 25% yield. M.p.= 142-143 ^{0}C; IR (film, $CHCl_3$) ν(cm^{-1}): 2021,1694, 1604, 1570, 1392, 1262, 955, 784; ^{1}H NMR ($CDCl_3$, 300 MHz): δ 1.62-1.69 (3H, m, H-4 and H-5), 2.17-2.30 (2H, m, H-5 and H-5a), 2.66 (1H, dd, *J* =6.5 and 10.9 Hz, H-6), 2.50 (1H, dd, *J* =6.5 and 11.0 Hz, H-6), 4.77 (1H, t, *J* =3.9 Hz, H-1a), 5.93-5.99 (1H, m, H-3), 6.04-6.09 (1H, m, H-3), 7.49 (1H, ddd, *J* = 1.2, 7.5 and 8.7 Hz,H-8), 7.63 (1H, ddd, *J* = 1.2, 7,5 and 9.0 Hz, H-9), 7.80 (1H, dd, *J* = 0.9 and 7.5 Hz, H-10), 8.05 (1H,

dd, *J* = 0.9 and 7.5 Hz, H-7); $^{13}C\{1H\}$ NMR ($CDCl_3$, 75 MHz): δ 22.5 (C-4), 23.6 (C-5), 24.7 (C-6), 29.3 (C-5a), 73.8 (C-1a), 112.2 (C-6a), 124.3 (C-3), 124.7 (C-2), 128,8, 130.8, 134.1 and 135.0 (C-ar), 130.2 (C-8a), 132.4 (C-12a), 161.6 (C-12b), 179.9 (2C=O); HRMS (ESI/Q-TOF) m/z: $[M + Na]^+$ Calcd for $C_{17}H_{14}O_3Na$ 289.0943; Found 289.0932. Anal. Calcd for $C_{17}H_{14}O_3$: C, 71.10; H, 5.22. Found: C, 71.09; H, 5.20.

2-phenyl-3,4-dihydro-2H-benzo[*g*]chromene-5,10-dione (10a).[22] Compound **10a** was obtained as a yellow solid in 80% yield (140 mg). M.p.= 168-170 ^{0}C; IR (film, $CHCl_3$) ν(cm^{-1}): 1679, 1649, 1617, 1260, 1202, 1063, 958, 910, 721; ^{1}H NMR ($CDCl_3$, 300 MHz): δ 2.15 (1H, dddd, *J* = 2.6, 3.2, 5.7 and 14.0 Hz, H-3a), 2.30 (1H, dddd, *J* = 2.2, 6.2, 6.5 and 14.0 Hz, H-3b), 2.63 (1H, ddd, *J* = 3.2, 6.2 and 13.7 Hz, H-4a), 2.77 (1H, ddd, *J* = 2.2, 5.7, and 13.7 Hz, H-4b), 5.22 (1H, dd, *J* = 2,6 e 6,5 Hz, H-2), 7.32 – 7.40 (5H, m, *2-phenyl*), 7.68 (2H, dddd, *J* = 2.0, 7.5, 9.2 and 11.0 Hz, H-8 e H-7), 8.10 (2H, dddd, *J* =2.0, 7.5, 9.2 and 10.9 Hz, H-9 e H-6); $^{13}C\{1H\}$ NMR ($CDCl_3$, 75 MHz): δ 18.3 (C-4), 27.6 (C-3), 78.8 (C-2), 121.4 (C-4a), 125.6 (C-4'-*phenyl*), 125.8 (C-6), 126.1 (C-9), 128.1 (C-2'-*phenyl*), 128.4 (C-3'-*phenyl*), 130.8 (C-9a), 131.7 (C-5a), 132.9 (C-7, C-8), 133.7 (C-Har), 139.1 (C-1'), 152.2 (C-10a), 184.0 (C-5 and C-10); HRMS (ESI/Q-TOF) m/z: $[M + Na]^+$ Calcd for $C_{19}H_{14}O_3Na$ 313.0943; Found: 313.0936. Anal. Calcd for $C_{19}H_{14}O_3$: C, 78.61; H, 4.86. Found: C, 78.70; H, 4.94.

2-phenyl-3,4-dihydro-2*H*-benzo[*h*]chromene-5,6-dione (10b).[22] Compound **10b** was obtained as an orange solid in 20% yield (35 mg). M.p.= 161-163 ^{0}C; IR (film, $CHCl_3$) ν(cm^{-1}): 1696, 1647, 1605,1573, 1397, 1300, 1280, 1232, 1158, 1093, 922, 700; ^{1}H NMR ($CDCl_3$, 300 MHz): δ 2.08 (1H, dddd, *J* = 2.7, 3.2, 5.6 and 13.8 Hz, H-3a), 2.33 (1H, dddd, *J* = 3.4, 6.3, 7.4 and 13.8 Hz, H-3b), 2.60 (1H, ddd, *J* = 3.2, 6.3 and 8.8 Hz, H-4a), 2.76 (1H, ddd, *J* = 3.4, 5.6 and 8.8 Hz, H-4b), 5.27 (1H, dd, *J* = 2.7 and 7.4 Hz, H-2), 7.39-7.46 (5H, m, 2-*phenyl*), 7.53 (1H, ddd, *J* = 1.0, 7.4 and 8.6 Hz, H-8), 7.64 (1H, ddd, *J* = 1.4, 7.6 and 9.1 Hz, H-9), 7.83 (1H, dd, *J* = 1.0 and 7.6 Hz, H-10), 8.01 (1H, dd, *J* = 1.4 and 7.6 Hz, H-7). $^{13}C\{1H\}$ NMR ($CDCl_3$, 75 MHz): δ 18.2 (C-4), 28.2 (C-3), 79.9 (C-2), 113.8 (C-4a), 123.9 (C-10), 125.6 (C-7), 125.7 (C-4'-*phenyl*), 128.4 (C-8), 128.5 (C-2'-*phenyl*), 128.6 (C-3'-*phenyl*), 129.8 (C-6a), 130.6 (C-9), 131.9 (C-1'-*phenyl*),

139.2 (C-10a), 162.7 (C-10b), 178.7 and 179.0 (C-5 and C-6); HRMS (ESI/Q-TOF) m/z: $[M + Na]^+$ Calcd for $C_{19}H_{14}O_3Na$ 313.0943; Found: 313.0944. Anal. Calcd for $C_{19}H_{14}O_3$: C, 78.61; H, 4.86. Found: C, 78.67; H, 4.91.

2-(4-fluorophenyl)-3,4-dihydro-2*H*-benzo[*g*]chromene-5,10-dione (11a).[29] Compound **11a** was obtained as a yellow solid in 75% yield (130 mg). M.p.= 171-173 ^{0}C; IR (film, $CHCl_3$) ν(cm^{-1}): 1678, 1647, 1618, 1513, 1260, 1201, 1065, 958, 835, 720; ^{1}H NMR ($CDCl_3$, 300 MHz): δ 2.15 (1H, dddd, *J* = 2.4, 3.3, 6.5 and 13.0 Hz, H-3a), 2.30 (1H, dddd, *J* = 2.1, 6.2, 7.0 and 13.0 Hz, H-3b), 2.75 (1H, ddd, *J* = 3.3, 6.2 and 12.5 Hz, H-4a), 2.80 (1H, ddd, *J* = 2.1, 6.5, and 12.5 Hz, H-4b), 5.16 (1H, dd, *J* = 2.4 and 7.0 Hz, H-2), 7.08 (2H, t, *J* = 8.7, 2Char-F), 7.36 – 7.41 (2H, m, 2ArH), 7.70 (2H, dddd, *J* = 1.5, 7.5, 9.2 and 11.0 Hz, H-8 and H-7), 8.10 (2H, dddd, *J* = 1.5, 7.5, 9.2 and 10.9 Hz, H-9 and H-6); ^{13}C{1H} NMR ($CDCl_3$, 75 MHz): δ 18.5 (C-4), 27.8 (C-3), 78.3 (C-2), 115.3 and 115.6 (d, *J* = 21.4 Hz, 2Char-F), 121.4 (C-4a), 125.9 (C-6), 126.2 (C-9), 127.5 (C-7), 127.6 (C-8), 133.0 (C-2'), 133.8 (C-3'), 130.8 (C-9a), 131.8 (C-5a), 135.0 (C-4'), 155.1 (C-10a), 179.1 and 184.0 (C-5 and C-10); HRMS (ESI/Q-TOF) m/z: $[M + Na]^+$ Calcd for $C_{19}H_{13}FO_3Na$ 331.0849; Found: 331.0838. Anal. Calcd for $C_{19}H_{13}FO_3$: C, 74.02; H, 4.25. Found: C, 74.09; H, 4.31.

2-(4-fluorophenyl)-3,4-dihydro-2*H*-benzo[*h*]chromene-5,6-dione (11b).[11] Compound **11b** was obtained as an orange solid in 25% yield (44 mg). M.p.= 142-147 ^{0}C; IR (film, $CHCl_3$) ν(cm^{-1}): 1573, 1607, 1513, 1394, 1280, 1229, 1156, 922; ^{1}H NMR ($CDCl_3$, 300 MHz): δ 2.07 (1H, dddd, *J* = 2.4, 3.2, 5.6 and 12.8 Hz, H-3a), 2.34 (1H, dddd, *J* = 3.1, 6.5, 7.8 and 12.8 Hz, H-3b), 2.61 (1H, ddd, *J* = 3.2, 6.5 and 8.7 Hz, H-4a), 2.75 (1H, ddd, *J* = 3.1, 5.6 and 8.7 Hz, H-4b), 5.24 (1H, dd, *J* = 2.4 and 7.8 Hz, H-2), 7.15 (2H, t, *J* = 8.5 Hz, 2Char-F), 7.39-7.44 (2H, m, H-ar), 7.53 (1H, ddd, *J* = 1.2, 7.2 and 8.7 Hz, H-8), 7.64 (1H, ddd, *J* = 1.4, 7.8 and 9.2 Hz, H-9), 7.83 (1H, dd, *J* = 1.1 and 6.5 Hz, H-10), 8.01 (1H, dd, *J* = 1.1 and 6.3 Hz, H-7). ^{13}C{1H} NMR ($CDCl_3$, 75 MHz): δ 18.3 (C-4), 28.3 (C-3), 79.4 (C-2), 113.8 (C-4a), 115.4 and 115.7 (d, *J* = 21.4 Hz, C-3'), 123.8 (C-10), 127.5 (C-7), 127.6 (C-8), 128.6 (C-1'), 129.8 (C-6a), 130.7 (C-3'), 131.8 (C-2'), 134.7 (C-9'), 135.7 (C-4'), 137.7 (C-10a), 162.6 (C-10b), 178.4 and 179.2 (C-5 and C-6); HRMS (ESI/Q-TOF) m/z: $[M + Na]^+$ Calcd for

$C_{19}H_{13}FO_3Na$ 331.0849; Found: 331.0845. Anal. Calcd for $C_{19}H_{13}FO_3$: C, 74.02; H, 4.25. Found: C, 74.00; H, 4.25.

2-(4-chlorophenyl)-3,4-dihydro-2*H*-benzo[*g*]chromene-5,10-dione (12a).[29] Compound **12a** was obtained as a yellow solid in 80% yield (140 mg). M.p.= 130-132 ^{0}C; IR (film, $CHCl_3$) ν(cm^{-1}): 3068, 2929,1677, 1650, 1620, 1597, 1260, 1202, 1065, 911, 823, 720; ^{1}H NMR ($CDCl_3$, 300 MHz): δ 1.97-2.10 (1H, m, H-3); 2.26-2.35 (1H, m, H-3); 2.59-2.80 (2H, m, H-4); 5.17 (1H, dd, *J* = 2.6 and 6.8 Hz, H-2); 7.29 – 7.39 (4H, m, ArH); 7.70 (2H, dddd, *J* = 2.1; 7.8; 9.2; 11.0 Hz, H-8 and H-7); 8.10 (2H, dddd, *J* = 2.0; 7.8; 9.2; 10.9 Hz, H-9 and H-6); ^{13}C{1H} NMR ($CDCl_3$, 75 MHz): δ 18.8 (C-4); 28.1 (C-3); 78.5 (C-2); 121.8 (C-4a); 126.3; 126.6; 127.5; 129.1; 133.4 and 134.2 (C-Har); 131.2 (C-9a); 132.1 ($\underline{C}_{ar}$-Cl); 134.4 (C-5a); 138.1 ($C_{quat.ar}$); 155.4 (C-10a); 184,4 (C=O); HRMS (ESI/Q-TOF) m/z: $[M + Na]^+$ Calcd for $C_{19}H_{13}ClO_3Na$ 347.0553; Found: 347.0542. Anal. Calcd for $C_{19}H_{13}ClO_3$: C, 70.27; H, 4.03. Found: C, 70.10; H, 4.08.

2-(4-chlorophenyl)-3,4-dihydro-2*H*-benzo[*h*]chromene-5,6-dione (12b).[11] Compound **12b** was obtained as an orange solid in 20% yield (35 mg). M.p.= 143-145 ^{0}C; IR (film, $CHCl_3$) ν(cm^{-1}): 3068, 2928, 1697, 1647, 1607, 1393, 1281, 1092, 923, 774; ^{1}H NMR ($CDCl_3$, 300 MHz): δ 1.97-2.11 (1H, m, H-3); 2.27-2.36 (1H, m, H-3); 2.54-2.65 (1H, m, H-4); 2.74 (1H, ddd, *J* = 3.1; 5.6 and 8.7 Hz H-4); 5.24 (1H, dd, *J* = 2.4 and 7.8 Hz, C-2); 7.36-7.45 (4H, m, H-ar); 7.53 (1H, ddd, *J* = 1.2, 7.5 and 8.5 Hz,H-8); 7.64 (1H, ddd, *J* = 1.4, 7.5 and 9.0 Hz, H-9), 7.83 (1H, dd, *J* = 1.2 and 7.8 Hz, H-10), 8.01 (1H, dd, *J* = 1.9 and 8.0 Hz, H-7); ^{13}C{1H} NMR ($CDCl_3$, 75 MHz): δ: 18.2 (C-4), 28.2 (C-3), 79.2 (C-2), 113.8 (C-4a), 123.8; 127.1; 128.6; 128.8; 130.7 and 134.8 (C-ar); 129.8 (C-6a); 131,9 (Cquart C-2); 134.2 (Car-Cl); 137.7 (C-10a); 162.5 (10b); 178.3 and 179,2 (2C=O); HRMS (ESI/Q-TOF) m/z: $[M + Na]^+$ Calcd for $C_{19}H_{13}ClO_3Na$ 347.0553; Found: 347.0542. Anal. Calcd for $C_{19}H_{13}ClO_3$: C, 70.27; H, 4.03. Found: C, 70.10; H, 4.08.

2-(4-methylphenyl)-3,4-dihydro-2*H*-benzo[*g*]chromene-5,10-dione (13a).[29] Compound **13a** was obtained as a yellow solid in 70% yield (122 mg). M.p.= 135-137 ^{0}C; IR (film, $CHCl_3$) ν(cm^{-1}): 2920,1677, 1645, 1617, 1595, 1258, 1200, 1065, 958, 826, 720; ^{1}H NMR ($CDCl_3$, 300 MHz): δ 2.01-2.14 (1H, m, H-3);

2.26-2.33 (1H, m, H-3); 2.36 (1H, s, C$\underline{H}_3$); 2.59-2.79 (2H, m, H-4); 5.18 (1H, dd, *J* = 2.6 and 6.3 Hz, H-2); 7.18 – 7.29 (4H, m, ArH); 7.69 (2H, dddd, *J* = 1.0; 7.3; 9.0; 10.7 Hz, H-8 and H-7); 8.09 (2H, dddd, *J* = 1.0; 7.3; 9.0; 10.7 Hz, H-9 and H-6); ^{13}C{1H} NMR ($CDCl_3$, 75 MHz): δ 18.8 (C-4); 21.4 ($\underline{C}H_3$); 28.0 (C-3); 79.2 (C-2); 121.8 (C-4a); 126.1; 126.2; 126.5; 129.5; 133.7 and 134.1 (C-Har); 131.3 (C-9a); 136.3 (C-5a); 138.3 (Cquat.ar); 155.8 (C-10a); 179.6 and 184,0 (2C=O); HRMS (ESI/Q-TOF) m/z: $[M + Na]^+$ Calcd for $C_{20}H_{16}O_3Na$ 327.1099; Found: 327.1103. Anal. Calcd for $C_{20}H_{16}O_3$: C, 78.93; H, 5.30. Found: C, 78.90; H, 5.28.

2-(4-methylphenyl)-3,4-dihydro-2*H*-benzo[*h*]chromene-5,6-dione (13b).[29] Compound **13b** was obtained as an orange solid in 30% yield (52 mg). M.p.= 165-167 ^{0}C; IR (film, $CHCl_3$) νcm^{-1}): 2924, 1697, 1647, 1590, 1572, 1393, 1280, 1151, 922, 771; ^{1}H NMR ($CDCl_3$, 300 MHz): δ: 2.00-2.14 (1H, m, H-3); 2.27-2.35 (1H, m, H-3); 2.40 (3H, s, C$\underline{H}_3$) 2.53-2.64 (1H, m, H-4); 2.77 (1H, ddd, *J* = 3.1; 5.6 and 8.7 Hz H-4); 5.24 (1H, dd, *J* = 2.4 and 7.8 Hz, C-2); 7.24-7.33 (4H, m, H-ar); 7.51 (1H, ddd, *J* = 1.4, 7.5 and 8.7 Hz, H-8); 7.62 (1H, ddd, *J* = 1.4, 7.5 and 9.0 Hz, H-9), 7.81 (1H, dd, *J* = 1.2 and 7.8 Hz, H-10); 8.01 (1H, dd, *J* = 1.4 and 7.5 Hz, H-7); ^{13}C{1H} NMR ($CDCl_3$, 75 MHz): δ: 18.7 (C-4); 21.4 ($\underline{C}H_3$); 28.6 (C-3); 80.4 (C-2); 114.3 (C-4a); 124.3; 126.1; 128.9; 129.7; 131.0 and 135.1 (C-ar); 130.2 (C-6a); 132.4 (Cquart-C-2); 136.7 (Car-CH_3); 138.7 (C-10a); 163.2 (10b); 178.8 and 179.8 (2C=O); HRMS (ESI/Q-TOF) m/z: $[M + Na]^+$ Calcd for $C_{20}H_{16}O_3Na$ 327.1099; Found: 327.1095. Anal. Calcd for $C_{20}H_{16}O_3$: C, 78.93; H, 5.30. Found: C, 78.90; H, 5.28.

2-(4-methoxyphenyl)-3,4-dihydro-2*H*-benzo[*g*]chromene-5,10-dione (14a). [29] Compound **14a** was obtained as a yellow solid in 80% yield (140 mg). M.p.= 165-166 ^{o}C; IR (film, $CHCl_3$) $\nu(cm^{-1})$: 1681, 1645, 1612, 1245, 1194, 1062, 1021, 953, 720; ^{1}H NMR ($CDCl_3$, 300 MHz): δ 2.10 (1H, dddd, *J* = 2.6, 3.5, 6.4 and 13.0 Hz, H-3°), 2.28 (1H, dddd, *J* = 2.0, 6.1, 6.3 and 13.0 Hz, H-3b), 2.59 (1H, ddd, *J* = 3.5, 6.1 and 12.2 Hz, H-4a), 2.76 (1H, ddd, *J* = 2.0, 6.4, and 12.2 Hz, H-4b), 5.14 (1H, dd, *J* = 2.6 and 6.3 Hz, H-2), 6.89 (2H, d, *J* = 8.3 Hz, ArH), 7.30 (2H, d, *J* = 8.3 Hz, ArH), 7.69 (2H, dddd, *J* = 1.5, 7.5, 9.0, 11.0 Hz, H-8 and H-7), 8.09 (2H, dddd, *J* = 1.5, 7.5, 9.0, 10.9 Hz, H-9 and H-6). ^{13}C{1H} NMR

($CDCl_3$, 75 MHz): δ 19.0 (C-4), 28.0 (C-3), 55.5 ($O\underline{C}H_3$), 79.1 (C-2), 114.3 (C-4a), 126.2 (C-6), 126.5 (C-9), 133.5 (C-7), 134.1 (C-8), 131.3 (C-9a), 131.7 (C-5a), 155.8 (C-10a), 159.9 (C-4'), 179.7 and 184.5 (C-5 and C-10); HRMS (ESI/Q-TOF) m/z: $[M + Na]^+$ Calcd for $C_{20}H_{16}O_4Na$ 343.1049; Found: 343.1041. Anal. Calcd for $C_{20}H_{16}O_4$: C, 74.99; H, 5.03. Found: C, 74.89; H, 5.07.

2-(4-methoxyphenyl)-3,4-dihydro-2*H*-benzo[*h*]chromene-5,6-dione (14b).[11] Compound **14b** was obtained as a yellow solid in 20% yield (35 mg). M.p.= 155-157 ^{0}C; IR (film, $CHCl_3$) ν(cm^{-1}): 1605, 1572, 1525, 1280, 1249, 1170, 921, 774; ^{1}H NMR ($CDCl_3$, 300 MHz): δ 2.11 (1H, dddd, *J* = 2.4, 3.6, 5.7 and 13.0 Hz, H-3a); 2.31 (1H, dddd, *J* = 3.2, 6.2, 7.8 and 13.0 Hz, H-3b); 2.61 (1H, ddd, *J* = 3.6, 6.2 and 8.7 Hz, H-4a), 2.76 (1H, ddd, *J* = 3.2, 5.7 and 8.7 Hz H-4b), 3.85 (3H, s, $O\underline{C}H_3$), 5.20 (1H, dd, *J* = 2.4 and 7.8 Hz, C-2), 6.96-6.99 (2H, m, H-ar), 7.34-7.37 (2H, m, H-ar), 7.51 (1H, ddd, *J* = 1.4, 7.5 and 8.7 Hz,H-8), 7.60 (1H, ddd, *J* = 1.4, 7.5 and 9.0 Hz, H-9), 7.80 (1H, dd, *J* = 1.2 and 7.8 Hz, H-10), 8.08 (1H, dd, *J* = 1.4 e 7.5 Hz, H-7). ^{13}C{1H} NMR ($CDCl_3$, 75 MHz): δ: 18.4 (C-4), 28.0 (C-3), 55.2 ($O\underline{C}H_3$), 79.9 (C-2), 113.8 (C-4a), 114.0 (C-10), 123.9 (C-7), 127.2 (C-8), 128.5 (C-2'), 129.8 (C-6a), 130.6 (C-3'), 131.2 (C-9'), 132.0 (C-10a), 134.7 (C-1'), 159,6 (C-4'), 162.9 (C-10b), 178.4 and 179.4 (C-5 and C-6). HRMS (ESI/Q-TOF) m/z: $[M + Na]^+$ Calcd for $C_{20}H_{16}O_4Na$ 343.1049; Found: 343.1054. Anal. Calcd for $C_{20}H_{16}O_4$: C, 74.99; H, 5.03. Found: C, 74.97; H, 5.01.

2-phenyl-4H-benzo[g]chromene-5,10-dione (15). Compound **15** was obtained as a yellow solid in 60% yield (104 mg). M.p.= 157-163 ^{0}C; IR (film, $CHCl_3$) ν(cm^{-1}): 3401, 2918, 1673, 1651, 1625, 1245, 1206, 1101, 998, 758; ^{1}H NMR ($CDCl_3$, 300 MHz): δ 3.36 (2H, d, *J* = 3.7 Hz, H-4), 5.68 (1H, t, *J* = 3.7 Hz, H-3), 7.35-7.43 (3H, m, H-8 and H-7 and H-*para* at C-2), 7.68-7.75 (4H, m, ArH), 8.09-8.16 (2H, m, H-9 and H-6); ^{13}C{1H} NMR ($CDCl_3$, 75 MHz): δ 21.9 (C-4), 100.5 (C-3), 121.6 (C-4a), 126.9, 128.5, 128.9, 131.0, 131.4, 135.9 and 136.6 (C-Har), 133.4 (C-5a), 134.2 (C-9a), 135.0 (C-quat. Ar), 150.7 (C-10a), 154.5 (C-2), 186.6 (C-5 and C10); HRMS (ESI/Q-TOF) m/z: $[M + Na]^+$ Calcd for $C_{19}H_{12}O_3Na$ 311.0786; Found: 311.0775. Anal. Calcd for $C_{19}H_{12}O_3$: C, 79.19; H, 4.20. Found: C, 79.10; H, 4.20.

Procedure for preparation of 10a/10b at large scale. To a round-bottom flask equipped with a magnetic stirring bar, 5 grams (28.71 mmols) of lawsone was dissolved in dioxane (100 mL), followed by addition of 6.89 grams of formaldehyde (229.68 mmol). The 8.97 grams of styrene (86.13 mmols) was added dropwise and the reaction mixture was stirred under reflux until consumption of the starting material. The solvent was removed under reduced pressure; ethyl acetate was added in the residue and the mixture was washed with saturated sodium bicarbonate aqueous solution. The combined organic extract was washed with water, dried over anhydrous sodium sulfate, filtered and concentrated under vacuum. The residual mixture of products was purified by flash chromatography employing gradient *n*-hexane/EtOAc as eluent, furnishing the desired 1,2-naphthoquinone (**10a**) and 1,4-naphthoquinone (**10b**) in 75% (3.7 grams) and 25% (1.3 grams) yields, respectively.

Computational details.

Full geometry optimizations were carried out using the hybrid DFT M06-2X functional[30] together with the 6-31+G(d,p) basis set. For each optimized stationary point, the second-order Hessian matrix was computed at the same level to confirm the stationary point as a minimum on the potential energy surface, in which all eigenvalues are positive, or a transition structure, with just one negative eigenvalue of the Hessian matrix. For each transition structure, the negative normal mode was animated to confirm that it connects the desired minima. Additionally, the distorted transition state structure obtained during the animation was optimized towards products and pre-reactive complexes. The normal mode calculations were also useful for computing the thermodynamic parameters at 298 K using standard statistical thermodynamic equations for an ideal gas[31]. Apart from the gas-phase calculations, solvation effects were also accounted for by using water and dioxane as implicit solvent within the polarized continuum solvation model (IEFPCM)[32,33]. All computations were performed with the G09 software package using default convergence criteria[34].

For the reaction between $\mathbf{4_H}$ and ethene, IRC calculations[35-37] from the transition state structures $\mathbf{TS_\alpha}$ and $\mathbf{TS_\beta}$ towards products (α- and β-lapachone, respectively) and pre-reactive complexes (**IC**) were performed. The transient structures obtained at each IRC point were decomposed into two fragments ($\mathbf{4_H}$

and ethene), which were used for subsequent Activation Strain Model calculations (ASM) [38,39] and Energy Decomposition (EDA)[40,41] analyses. Energy Decomposition Analysis (EDA) was performed using the GAMESS *ab initio* quantum chemistry package[42], according to the Morokuma-Kitaura decomposition scheme[43], in which the interaction energy (E_{int}) between two closed shell monomers (fragments) is decomposed into five components: electrostatic, Pauli repulsion, polarization, exchange, and dispersion energy terms (E_{ES}, E_{REP}, E_{POL}, E_{EX} and E_{DISP}, respectively). Additionally, the final comparison of interaction between the triplet acrolein diradicals shown in **Table 4** was performed by single-point energy calculations of the open shell triplet acrolein diradicals using G09 software[31].

SUPPORTING INFORMATION

Cartesian coordinates of the optimized structures (minima and transition states) in the gas phase; ^{1}H- and ^{13}C{1H}-NMR spectra of the compounds.

ACKNOWLEDGMENT

The authors would like to acknowledge CNPq (grants no. 309080/2015-0 and 434955/2018-3), FAPERJ (grants no. E-26/203.001/2017, E-26/010.101118/2018 and E-26010.001424/2019), and CAPES PRINT Program (Process No. 88881.310460/2018-01).

REFERENCES

1. Nielsen, C. D.-T.; Abas, H.; Spivey, A. C. Stereoselective Reactions of ortho-Quinone Methide and ortho-Quinone Methide Imines and Their Utility in Natural Product Synthesis. *Synthesis* **2018**, *50*, 2018, 4008-4018.

2. Wang, Z.; Sun, J. Recent Advances in Catalytic Asymmetric Reactions of o-Quinone Methides. *Synthesis* **2015**, *47*, 3629-3644.

3. Caruana, L.; Fochi, M. F.; Bernardi, L. The Emergence of Quinone Methides in Asymmetric Organocatalysis. *Molecules*, **2015**, *20*, 11733-11764.

4. Pathak, T. P.; Sigman, M. S. Applications of ortho-Quinone Methide Intermediates in Catalysis and Asymmetric Synthesis. *J. Org. Chem.* **2011**, *76*, 9210-9215.

5. Yanga, B.; Gao, S. Recent advances in the application of Diels–Alder reactions involving o-quinodimethanes, aza-o-quinone methides and o-quinone methides in natural product total synthesis. *Chem. Soc. Rev.* **2018**, *47*, 7926-7953.

6. Willis, N. J.; Bray, C. D. Ortho-Quinone Methides in Natural Product Synthesis. *Chem. Eur. J.* **2012**, *18*, 9160-9173.

7. Barta, P.; Fülöp, F.; Szatmári, I. Mannich base-connected syntheses mediated by ortho-quinone methides. *Beilstein J. Org. Chem.* **2018**, *14*, 560-575.

8. Jordão, A. K.; Vargas, M. D.; Pinto, A. C.; da Silva, F. C.; Ferreira, V. F. Lawsone in organic synthesis. *RSC Adv.* **2015**, *5*, 67909-67943.

9. Cardoso, M. F. C.; Forezi, L. S. M.; Cavalcante, V. G. S.; Juliani, C. S. R.; Resende, J. A. L. C.; da Rocha, D. R.; da Silva, F. C.; Ferreira, V. F. Synthesis of New Xanthenes Based on Lawsone and Coumarin via a Tandem Three Component Reaction. *J. Braz. Chem. Soc.* **2017**, *28*, 1926-1936.

10. Bala, B. D.; Rajesh, S. M.; Perumal, S. An eco-friendly sequential catalyst- and solvent-free four-component stereoselective synthesis of novel 1,4-pyranonaphthoquinones. *Green Chem.* **2012**, *14*, 2484-2490.

11. Ferreira, S. B.; Salomão, K.; da Silva, F. C.; Pinto, A. V.; Kaiser, C. R.; Pinto, A. C.; Ferreira, V. F.; de Castro, S. L. Synthesis and anti-Trypanosoma cruzi activity of b-lapachone analogues. *Eur. J. Med. Chem.* **2011**, 46, 3071-3077.

12. Carneiro, P. F.; Pinto, M. C. F. R.; Marra, R. K. F.; Campos, V. R.; Resende, J. A. L. C.; Delarmelina, M.; Carneiro, J. W. M.; Lima, E. S.; da Silva, F. C. ; Ferreira, V. F. Insight into and Computational Studies of the Selective Synthesis of 6H Dibenzo[b,h]xanthenes. *J. Org. Chem.* **2016**, *81*, 5525-5537.

13. Osipov, D. V.; Osyanin, V. A.; Klimochkin, Y. N. ortho-Quinone methides as key intermediates in cascade heterocyclizations. *Russ. Chem. Rev.* **2017**, *86*, 625-687.

14. Jaworski, A. A.; Scheidt, K. A. Emerging Roles of in Situ Generated Quinone Methides in Metal-Free Catalysis. *J. Org. Chem.* **2016**, *81*, 10145-10153.

15. Singh, M. S.; Nagaraju, A.; Anand, N.; Chowdhury, S. ortho-Quinone methide (o-QM): a highly reactive, ephemeral and versatile intermediate in organic synthesis. *RSC Adv.* **2014**, *4*, 55924-55959.

16. Basari, N.; Majerskia, K. M.; Kralj, M. Quinone Methides: Photochemical Generation and its Application in Biomedicine. *Curr. Org. Chem.* **2014**, *18*, 3-18.

17. Bolton, J. L. Quinone Methide Bioactivation Pathway: Contribution to Toxicity and/or Cytoprotection? *Curr. Org. Chem.* **2014**, *18*, 61-69.

18. Li, Q.; Dong, T.; Liu, X.; Zhang, X.; Yang, X., Lei, X. Ortho-Quinone Methide Finds Its Application in Bioorthogonal Ligation. *Curr. Org Chem.* **2014**, *18*, 86-92.

19. Cardoso, M. F. C.; Forezi, L. S. M.; Cavalcante, V. G. S.; Juliani, C. S. R.; Resende, J. A. L. C.; Rocha, D. R.; da Silva, F. C.; Ferreira, V. F. Synthesis of New Xanthenes Based on Lawsone and Coumarin via a Tandem Three Component Reaction. *J. Braz. Chem. Soc.* **2017**, *28*, 1926-1936.

20. Jordão, A. K.; Vargas, M. D.; Pinto, A. C.; da Silva, F. C.; Ferreira, V. F. Lawsone in organic synthesis. *RSC Adv.* **2015**, *5*, 67909-67943.

21. Forezi, L. S. M.; Marra, R. K. F.; Silva, F. C.; Ferreira, V. F. Synthetic Strategies for Obtaining Xanthenes. *Curr. Org. Syn.* **2017**, *14*, 929-951.

22. da Silva, F. C.; Ferreira, S. B.; Kaiser, C. R.; Pinto, A. C.; Ferreira, V. F. Synthesis of α- and β-lapachone derivatives from hetero diels-alder trapping of alkyl and aryl o-quinone methides. *J. Braz. Chem. Soc.* **2009**, *20*, 1478-1482.

23. Rocha, D. R.; Mota, K.; Silva, I. M. C. B.; Ferreira, V. F.; Ferreira, S. B.; Silva, F. C. Synthesis of fused chromene-1,4-naphthoquinones via ring-closing metathesis and Knoevenagel-electrocyclization under acid catalysis and microwave irradiation. *Tetrahedron*. **2014**, *70*, 3266-3270.

24. Wang, H.; Wang, Y.; Han, K.-L.; Peng, X.-J. A DFT Study of Diels-Alder Reactions of o-Quinone Methides and Various Substituted Ethenes: Selectivity and Reaction Mechanism. *J. Org. Chem.* **2005**, *70*, 4910-4917.

25. Peng, D.-Q.; Liu, Y.; Lu, Z.-F.; Shen, Y.-M.; Xu, J.-H. Synthesis of Siloxy-a-Lapachone Derivatives by Chemo- and Regioselective Diels–Alder Reactions of 3-Methylene-1,2,4-naphthotriones with Silyl Enol Ethers. *Synthesis*. **2008**, *8*, 1182-1192.

26. Hammond, G. S. A Correlation of Reaction Rates. *J. Am. Chem. Soc.* **1955**, *77*, 334-338.

27. von Hopffgarten, M.; Frenking, G. Energy Decomposition Analysis. *WIREs Comput. Mol. Sci.* **2012**, *2*, 43-62.

28. Zhao, L.; Hermann, M.; Schwarz, W. H. E.; Frenking, G. The Lewis electron-pair bonding model: modern energy decomposition analysis. *Nature Rev. Chem.* **2019**, *3*, 48-63.

29. Da Costa, Emmerson C. B.; Amorim, Raquel; Da Silva, Fernando C.; Rocha, David R.; Papa, Michelle P.; De Arruda, Luciana B.; Mohana-Borges, Ronaldo; Ferreira, V. F.; Tanuri, Amilcar; Da Costa, Luciana J.; Ferreira, S. B. Synthetic 1,4-Pyran Naphthoquinones Are Potent Inhibitors of Dengue Virus Replication. *Plos One*, **2013**, *8*, e82504.

30. Zhao, Y.; Truhlar, D. G. The M06 suite of density functionals for main group thermochemistry, thermochemical kinetics, noncovalent interactions, excited states, and transition elements: two new functionals and systematic testing of four M06-class functionals and 12 other function. *Theo. Chem. Acc.* **2008**, *120*, 215-241.

31. McQuarie, D. A.; Simon, J. D. Physical Chemistry: A Molecular Approach. California: University Science Book, **1997**.

32. Mennucci, B.; Cances, E.; Tomasi, J. Evaluation of Solvent Effects in Isotropic and Anisotropic Dielectrics and in Ionic Solutions with a Unified Integral Equation Method: Theoretical Bases, Computational Implementation, and Numerical Applications. *J. Phys. Chem. B.* **1997**, *101*, 10506-10517.

33. Tomasi, J.; Mennuci, B.; Cances, E. The IEF version of the PCM solvation method: an overview of a new method addressed to study molecular solutes at the QM ab initio level. *J. Mol. Struct. (Teochem)*. **1999**, *464*, 211-226.

34. Frisch, M. J.; Trucks, G. W.; Schlegel, H. B.; Scuseria, G. E.; Robb, M. A.; Cheeseman, J. R.; Scalmani, G.; Barone, V.; Mennucci, B.; Petersson, G. A.; Nakatsuji, H.; Caricato, M.; Li, X.; Hratchian, H. P.; Izmaylov, A. F.; Bloino, J.; Zheng, G.; Sonnenberg, J. L.; Hada, M.; Ehara, M.; Toyota, K.; Fukuda, R.; Hasegawa, J.; Ishida, M.; Nakajima, T.; Honda, Y.; Kitao, O.; Nakai, H.; Vreven, T.; Montgomery, J. A., Jr.; Peralta, J. E.; Ogliaro, F.; Bearpark, M.; Heyd, J. J.; Brothers, E.; Kudin, K. N.; Staroverov, V. N.; Keith, T.; Kobayashi, R.; Normand, J.; Raghavachari, K.; Rendell, A.; Burant, J. C.; Iyengar, S. S.; Tomasi, J.; Cossi, M.; Rega, N.; Millam, J. M.; Klene, M.; Knox, J. E.; Cross, J. B.; Bakken, V.; Adamo, C.; Jaramillo, J.; Gomperts, R.; Stratmann, R. E.; Yazyev, O.;

Austin, A. J.; Cammi, R.; Pomelli, C.; Ochterski, J. W.; Martin, R. L.; Morokuma, K.; Zakrzewski, V. G.; Voth, G. A.; Salvador, P.; Dannenberg, J. J.; Dapprich, S.; Daniels, A. D.; Farkas, O.; Foresman, J. B.; Ortiz, J. V.; Cioslowski, J.; Fox, D. J. Gaussian 09, revision D.01; Gaussian, Inc.: Wallingford, CT, 2013.

35. Fukui, K. Formulation of the reaction coordinate. *J. Phys. Chem.* **1970**, *74*, 4161-4163.

36. Fukui, K. The path of chemical reactions - the IRC approach. *Acc. Chem. Res.* **1981**, *14*, 363-368.

37. Garrett, B. C.; Redmon, M. J.; Steckler, R.; Truhlar, D. G.; Baldridge, K. K.; Bartol, D.; Schmidt, M. W.; Gordon, M. S. Algorithms and accuracy requirements for computing reaction paths by the method of steepest descent. *J. Phys. Chem.* **1988**, *92*, 1476-1488.

38. Bickelhaupt, F. M. Understanding reactivity with Kohn–Sham molecular orbital theory: E2–SN2 mechanistic spectrum and other concepts. *J. Comp. Chem.* **1999**, *20*, 114-128.

39. van Zeist, W.-J.; Bickelhaupt, F. M. The activation strain model of chemical reactivity. *Org. Biomol. Chem.* 2010, 8, 3118-3127.

40. Morokuma, K. Molecular orbital studies of hydrogen. *J. Chem. Phys.* **1971**, *55*, 1236-1244.

41. Ziegler, T.; Rauk, A. On the calculation of bonding energies by the Hartree–Fock Slater method. *Theor. Chim. Acta.* **1977**, *46*, 1-10.

42. Schmidt, M. W.; Baldridge, K. K.; Boatz, J. A.; Elbert, S. T.; Gordon, M. S.; Jensen, J. H.; Koseki, S.; Matsunaga, N.; Nguyen, K. A.; Su, S. J.; Windus, T. L.; Dupuis, M.; Montgomery, J. A.; *J. Comput. Chem.* **1993**, *14*, 1347-1363.

43. Kitaura, K.; Morokuma, K. A new energy decomposition scheme for molecular interactions within the Hartree-Fock approximation. *Intern. J. Quantum Chem.* **1976**, *10*, 325–340.

Graphical Abstract